Determination of the pharmacodynamic substances and mechanism of Shiwuwei Saierdou Pills against cholestatic hepatitis through chemical profile identification and network pharmacology analysis

Jing Qin [a], Gelin Xiang [a], Huimin Gao [b], Xianli Meng [c], Shaohui Wang [a,d,*], Yi Zhang [a,d,*]

[a] *State Key Laboratory of Southwestern Chinese Medicine Resources, School of Ethnic Medicine, Chengdu University of Traditional Chinese Medicine, Chengdu 611137, China*
[b] *State Key Laboratory of Southwestern Chinese Medicine Resources, School of Pharmacy, Chengdu University of Traditional Chinese Medicine, Chengdu 611137, China*
[c] *State Key Laboratory of Southwestern Chinese Medicine Resources, Innovative Institute of Chinese Medicine and Pharmacy, Chengdu University of Traditional Chinese Medicine, Chengdu 611137, China*
[d] *Meishan Hospital of Chengdu University of Traditional Chinese Medicine, Meishan 620010, China*

ARTICLE INFO

ABSTRACT

Cholestatic hepatitis (CH) is a liver lesion caused by abnormal bile production, secretion and excretion and has a complex pathogenesis. The Tibetan medicine Shiwuwei Saierdou Pills (SSP) is an empirical Tibetan medicine formula for the treatment of CH, but its chemical composition is complex and the material basis of its efficacy is not yet clear. So, in this study, the main chemical constituents and its blood-incorporated constituents in SSP were analyzed by ultra-high-performance liquid chromatography-quadruple-electrostatic field orbitrap high resolution mass spectrometry (UHPLC-Q-Exactive Orbitrap/MS), Then, the blood-incorporated constituents were subjected to network pharmacology analysis to preliminarily clarify its potential pharmacological substances and mechanism. and further, it was verified through molecular docking and *in vivo* animal experiments. As a result, a total of 80 chemical components were identified in the SSP, of which 11 were confirmed by reference standards and 20 blood-incorporated constituents (including 10 prototypes and 10 metabolites) were characterized in the serum containing the medicine. The core targets of SSP for the treatment of CH were identified as AKT1, VEGFA, CASP3, SRC and MAPK3 through the screening of the relationship between the blood-incorporated constituents and the targets. Combined with the results of molecular docking, swertiamarin, ellagic acid, taurocholic acid and bellidifolin in the ten prototypes may be the key pharmacodynamic substances for SSP to treat CH. The results of animal experiments showed that SSP could significantly inhibit the pathological changes of the CH rat model, and inhibit the protein expression of AKT1, VEGFA, CASP3, SRC and MAPK3. In summary, we used network pharmacology, molecular docking and animal experiments to preliminarily determine the main medicinal components, targets and pathways of SSP in the treatment of CH, which provides a scientific basis for further revealing the material basis and mechanism of SSP in treating CH.

1. Introduction

Hepatitis, a prevalent hepatic disorder, is categorized into jaundiced and non-jaundiced types based on the manifestation of jaundice, with cholestatic hepatitis (CH) constituting 2 % to 8 % of the jaundiced cases (Yang and Wang, 2021). CH, also termed biliary or bile duct hepatitis, encompasses a spectrum of liver pathologies instigated by diverse etiological factors. Disruptions at any stage of bile processing-from formation to excretion-might precipitate bile stasis, potentially escalating to hepatic impairment (Lindholm et al., 2022). Correspondingly, epidemiological investigations in China report that over 10 % of chronic liver disease hospital admissions are attributed to CH (Fang et al., 2020). Early detection of cholestasis is challenging; often, clinical findings include nonspecific symptoms alongside raised serum markers of ALP and GGT (Boyer, 2013, Lindholm et al., 2022). Cholestasis has no fixed group and can occur in any population and is generally benign(Li et al., 2020b). While CH may appear in any demographic and often has a benign course, protracted and intense bile obstruction can severely disrupt enterohepatic circulation, advancing toward fibrosis, cirrhosis, carcinomas, and eventual mortality (Han and Tian, 2016). Global mortality from viral hepatitis surpasses a million annually (Li et al., 2018), yet the only drug currently approved by the FDA for the treatment of cholestasis is ursodeoxycholic acid (2015). Hence, novel therapeutic strategies for CH require exploration.

The Shiwuwei Saierdou Pills (SSP) of Tibetan medicine is a compound formulation derived from the empirical amalgamation of two traditional Tibetan remedies: Bawei Zhangyacai Pills and Wuwei Jinse Pills. Chronicled within the seminal Tibetan medical text, 'Lan Liu Li', the Bawei Zhangyacai concoction is heralded for its efficacy in treating biliary tumors within the small intestine, espousing a therapeutic approach that induces clear evacuation of the bowels. Concurrently, the Wuwei Jinse Pills are traditionally prescribed by Tibetan practitioners to alleviate jaundiced hepatitis. The synergistic combination of these two formulas is applied to address an array of hepato-biliary ailments, including hepatic fever, cholecystitis, obstruction of the common bile duct, and cholelithiasis (Pan et al., 2021). Comprising a blend of fifteen fifteen herbs: *Swertiae chirayitae Herba, Chrysosplenii Herba, Nitroum, Hypecoe Herba, Lagotis Herba, Aconiti tangutici Herba, Punicae granati Semen, Herpetospermi Semen, Berberidis Cortex, Trogopteri Faeces, Saussureae Herba, Scrofa Faeces, Vladimiriae Radix, Chebulae Fructus and Vermiculitum*, SSP represents a complex herbal ensemble. The intricate nature of its phytochemical constitution poses challenges in deciphering the precise foundational components responsible for its purported therapeutic impacts, thus hindering broader.

Serological pharmacological profiling is a potent approach to rapidly discern the biologically active components of Chinese medicinal formulations following oral administration. This process entails tracing and characterizing the metabolites present in systemic circulation, thereby reflecting the distinctive pharmacokinetic properties of orally-administered Chinese medicinal therapies. The Q-Exactive system, founded upon Orbitrap technology, integrates a highly selective quadrupole for ion filtration with high-resolution, precise mass measurement, yielding an analytical method that is both highly discriminating and sensitive (Zhu et al., 2020, Zhang et al., 2021). Network pharmacology extends the boundaries of pharmacological research by mapping drug actions and disease mechanisms within expansive biological networks, underpinned by principles of systems biology (Li et al., 2022a). Concurrently, molecular docking provides an in silico platform for drug screening, efficiently delineating possible molecular targets for pharmaceutical compounds. The intricate nature of Tibetan medicinal formulations poses challenges due to their complex chemical constitution and the pleiotropy of their pharmacological targets (Zhang et al., 2019). This complexity is compounded by the paucity of investigations into the foundational material contributors to their therapeutic efficacy. To bridge this knowledge gap, we amalgamated network pharmacology with molecular docking strategies to unravel the specific pathways

through which SSP exert therapeutic effects in the context of CH. This multidisciplinary inquiry aspires to furnish a more rigorous scientific rationale for employing SSP in treating CH.

In this investigation, we conducted a comprehensive analysis of the chemical constituents of SSP both *in vitro* and in the plasma of rats post-gavage administration. Utilizing ultra-high-performance liquid chromatography-quadruple-electrostatic field orbitrap high resolution mass spectrometry (UHPLC-Q-Exactive Orbitrap/MS), we were able to identify and categorize the intricate array of bioactive compounds. Building on these findings, a network pharmacology approach was employed to elucidate the potential biological targets and pathways influenced by SSP's components. Key molecular targets were then subjected to further validation through the use of molecular docking techniques and *in vivo* experimental models (Fig. 1). The outcomes of this research lay the groundwork for a deeper understanding of the active substances within SSP and their corresponding mechanisms of action, contributing valuable scientific insights. Moreover, these findings underpin the pharmacological validation required for the broader clinical application of SSP as a treatment modality for CH.

2. Materials and methods

2.1. Main instruments

Vanquish Ultra Performance Liquid Chromatography coupled with Q Exactive Quadrupole-Electrostatic Field Orbital Trap High Resolution Mass Spectrometer (Thermo Fisher Scientific, USA); Waters Acquity UPLC HSS T3 C_{18} (2.1 mm × 100 mm,1.8 μm); Electronic Analytical Balance Type BSA124S (Beijing Sartorius Scientific Instruments Co., Ltd., Beijing, China); SB-8200DTS Type Dual Frequency Ultrasound Instrument (Ningbo Xingyi Ultrasound Equipment Co., Ltd., Ningbo, China); TGL-16 M benchtop high-speed frozen centrifuge (Changsha Xiangyi Centrifuge Instrument Co., Ltd., Changsha, China); XW-80A Vortex Mixer (Shanghai Chitang Electronics Co., Ltd., Shanghai, China); UPH-I-10 T UPP Series Ultra Pure Water Machine (Sichuan UPP Ultra Pure Technology Co., Ltd., Chengdu, China); JCS-110020 electronic balance (Harbin Zhong Hui Weighing Instrument Co., Ltd., Haerbing, China); FC-9 Enzyme Labeler (Shanghai Meigu Molecular Instruments, Shanghai, China).

2.2. Main drugs and reagents

SSP (Guomadian Z20026038, Batch No. 20201002) was provided by Qinghai Jiumei Tibetan Medicine Pharmaceutical Co. Ltd. (Xining, China). Protopine (batch no. DSTDY011301, purity ≥ 98 %), Coptisine (batch no. DST201105-003, purity ≥ 98 %), Gallic acid (batch no. DSTDM000801, purity ≥ 98 %), Ellagic acid (batch no. DSTDR000401, purity ≥ 98 %), Dehydrocostus lactone (batch no. DSTDQ004201, purity ≥ 98 %), Costunolide (batch no. DSTDM003002, purity ≥ 98 %), Mangiferin (batch no. DST200719-031, purity ≥ 98 %), Swertiamarin (batch no. DST201020-003, purity ≥ 98 %), Quercetin (batch no. DSTDH002802, purity ≥ 98 %), Hordenine (batch no. DST210615-041, purity ≥ 98 %), Scopoletin (batch no. DST210930-064, purity ≥ 98 %) were obtained from Chengdu Desite Biotechnology Co. Ltd. (Chengdu, China); α-naphthyl isothiocyanate (ANIT), Ursodeoxycholic acid (UDCA), Peanut oil, were obtained from Shanghai Yi'en Chemical Technology Co. Ltd. (Shanghai, China).

2.3. Experimental animals

Specific pathogen free (SPF) grade male SD rats, weight (200 ± 20) g, provided by Chengdu Dashuo Experimental Animal Co. (Animal Licence No. SCXK (Chuan) 2020–030) and from Hunan Enswell Laboratory Animals Co Ltd (Production Certificate No. SCXK(Xiang) 2019–0004). All rats were housed for 7 days in 12 h of light and 12 h of darkness, at 23 ± 2 °C and 40 %-70 % humidity, with free access to food

I. Component analysis

In vitro and *in vivo* composition analysis

II. Data collection

Collection of SSW blood entry component targets

Collection of disease targets
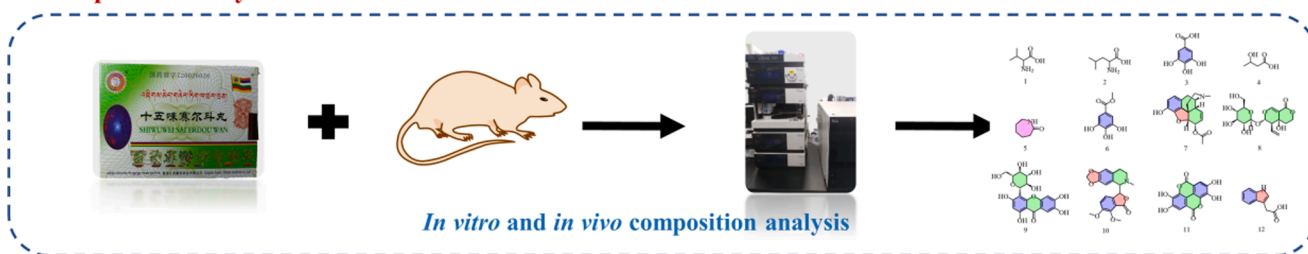
III. Network construction

IV. Network analysis

Enrichment pathway of 15 core targets

VEGFA signaling pathway

Molecular docking
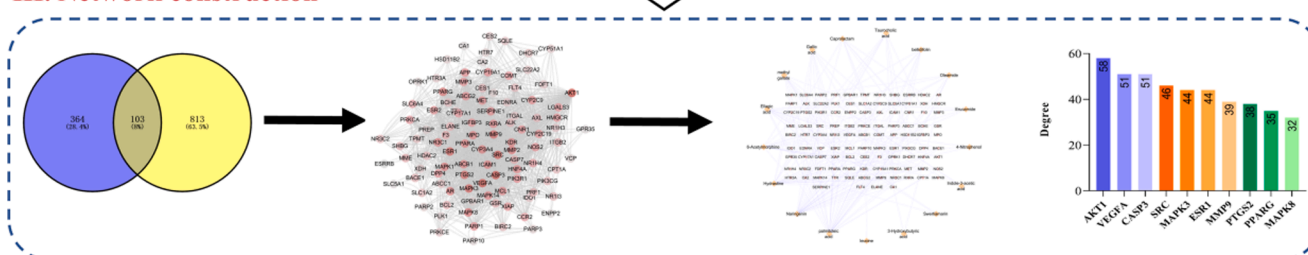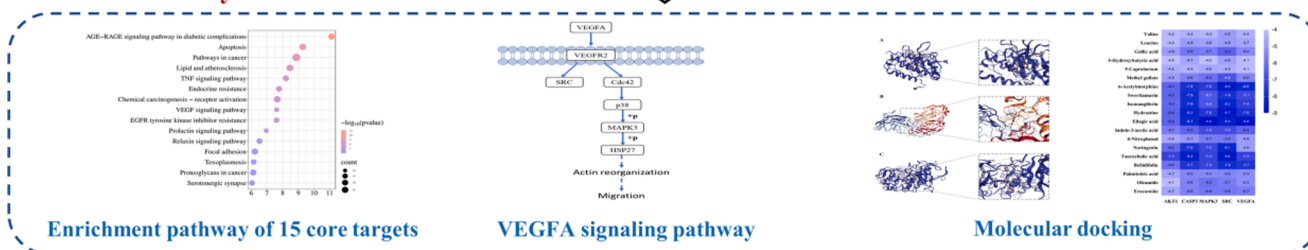
V. Experimental verification

Histopathological section of liver

Immunohistochemistry

Fig. 1. The workflow of research on the pharmacodynamic substances and mechanism of SSP in treating CH.

and water. The animals were fasted for 12 h before administration and were not water fasted throughout. All animals were housed in the animal house of Chengdu University of Traditional Chinese Medicine, NO: TCM-09–315, Laboratory Animal License No. SYXK(Chuan)2020–124.

2.4. Chromatographic conditions

Chromatographic columns: Waters Acquity UPLC HSS T3 C_{18} (2.1 mm × 100 mm, 1.8 μm); Mobile phase: 0.1 % formic acid aqueous solution (A) − 0.1 % formic acid acetonitrile solution (B); gradient elution: (0 ~ 48 min, 5%B ; 48 ~ 55 min, 95 %B); Flow rate: 0.3 ml/min; Column temperature: 35℃; Injection volume: 2 μl. The retention time

tolerances for this experiment were all in the range of 0.5 min.

2.5. Mass spectrometry conditions

Electrospray ionisation sources (ESI), Positive ion/negative ion scanning mode, Spray voltage: 3500 V(+) / 3500 V(-), Ion transfer tube temperature: 320 °C, Auxiliary gas heating temperature: 350 °C, Auxiliary gas flow rate: 10arb, Sheath gas flow rate: 35arb, Scan mode: Full MS dd-MS^2, Full MS resolution: 35000, dd-MS^2 resolution: 17500, Scan range: 100 ~ 1500, Collision energy gradients: 20, 40, 60 eV.

2.6. Preparation of control solutions

Precise weigh the amount of protopine, coptisine, gallic acid, ellagic acid, costunolide, mangiferin, swertiamarin, quercetin, hordenine, scopoletin, dehydrocostus lactone, add chromatographic methanol to 10 ml, weigh, sonicate for 30 min, weigh again and make up the weight to obtain the mixed standard solution.

2.7. Preparation of the test solution

Take about 0.3 g of SSP powder and weigh it precisely. Place it in a 50 ml conical flask, add 10 ml of chromatographic methanol, weigh the mass, sonicate for 30 min, weigh again, make up the lost mass with chromatographic methanol and shake well. The liquid is packed in 1.5 ml EP tubes and centrifuged for 5 min and the supernatant was passed through a 0.22 μm microporous membrane and the filtrate was renewed to obtain the test solution.

2.8. Preparation of the gavage solution

SSP powder, dissolved in pure water to a concentration 10 and 20 times the clinical dosing concentration (1.35 g/10 ml/kg, 2.7 g/10 ml/kg, converted from 1.5 g of SSP for a single dose in 70 kg of human body), for serum medicinal chemistry tests.

SSP powder was dissolved in saline into high (0.95 g/kg), medium (0.47 g/kg) and low (0.24 g/kg) doses (equivalent to 2, 1 and 0.5 times the daily clinical dosage in humans, based on a single dose of 1.5 g of SSP for 60 kg of human body) and used in network pharmacological validation experiments.

2.9. Group dosing and sample collection

For the experiments on the analysis of blood-incorporated constituents in SSP, six male SPF grade SD rats were randomly divided into three groups of two rats each. The control cohort received purified water, while the two treatment cohorts were administered either 10-fold or 20-fold concentrations of SSP via gavage at a dosage of 10 ml/kg. The dosing regimen spanned three days, consisting of morning, afternoon, and evening administrations, with a mandated 12-hour fasting period prior to the final dose, although water access remained unrestricted. Pursuant to the final gavage, and in compliance with approved ethical guidelines, blood collection was performed via the orbital plexus under deep anaesthesia to ensure a humane endpoint for each animal. These samples were collected at specified time points (15, 30, 45, 60, 90, 120, 180, 240, and 360 min post-administration) into heparinized 1.5 ml microcentrifuge tubes, centrifuged at 4000 rpm for 15 min at 4 °C. The resultant plasma was then stored at −80 °C for downstream *in vivo* chemical composition analysis.

For *in vivo* animal validation experiments, thirty-six SPF grade SD male rats were randomly divided into 6 groups: normal group, model group, SSW high, medium and low dose group and positive drug group (ursodeoxycholic acid). Rats were dosed at 10 ml/kg once a day for 7 days. After gavage on day 5 of the dosing period, at an interval of 4 h, all groups except the normal group were moulded by gavage with 100 mg/kg ANIT, and the normal group was gavaged with the same volume of

peanut oil, and then the dosing was continued at the original dose. Liver tissue was taken from each animal and placed in saline, rinsed to remove excess blood, blotted dry with filter paper and fixed in 4 % paraformaldehyde fixative, dehydrated, paraffin embedded and stained with HE for histopathological sections as well as immunohistochemical studies. The rats were anaesthetized by intraperitoneal injection of 1 % sodium pentobarbital saline solution at a dose of 35 mg/kg in all the above experiments.

2.10. Plasma sample processing

Add 200 μl of plasma, add 3 times the volume of acetonitrile to precipitate the protein, vortex for 3 min, centrifuge at 12,000 r/min for 20 min at 4 °C. Aspirate the supernatant, blow dry under nitrogen at 37 °C, add 200 μl of methanol to the residue, vortex for 3 min, centrifuge at 12,000 r/min at 4 °C, aspirate the supernatant and keep it for the sample. Blank plasma and administered plasma were operated according to this method.

2.11. Data processing

Raw liquid mass data was imported into Compound Discoverer 3.1 and a workflow was established for the identification of unknown compounds with primary and secondary mass deviations of < 5 ppm. The exact mass numbers and molecular formulae of the compounds were obtained from the mass-to-charge ratios of the primary excimer ion peaks, and then combined with the information of the secondary fragment ions, MassFrontier software, mzCloud web database, mzVault local Chinese medicine composition database search and reported literature as well as some of the controls, to analyse and identify the chemical composition of SSP and rat plasma samples. The chemical composition of the pills and rat plasma samples were analyzed and identified.

2.12. Network pharmacological analysis of 20 blood-incorporated constituents

Utilizing the ChemSpider database, molecular files in the 'MOL' format for components that entered the bloodstream were retrieved for analysis of serum samples from rats administered SSP via gavage. Subsequent target prediction for these bioactive molecules was carried out through the SwissTargetPrediction (https://swisstargetprediction.ch/) platform. After removing duplicate targets, the analysis yielded pertinent targets (relevance score > 0) for 20 blood-incorporated constituents. To identify targets associated with CH, a query was performed using the Gene Cards (https: //https://www.genecards.org/) and OMIM (https://omim.org/) databases, from which a curated list of relevant targets was compiled.

The data pertaining to targets associated with both the bioactive components of SSP and CH were integrated using Venny 2.1, which facilitated the identification of overlapping targets. These shared targets between the pharmacological agents and disease states were further analyzed on the STRING database by selecting "multiple proteins" and specifying the species as "Homo sapiens" This process enabled the acquisition of STRING (https://string-db.org/) derived information to construct the protein–protein interaction (PPI) network. The resulting data was imported into Cytoscape 3.9.1 and GraphPad Prism 9.2.0 software suites for graphical representation.

Pathway enrichment analysis was subsequently conducted with the intersecting targets using the DAVID 2021 (Dec. 2021) database. The parameters for this analysis were set to OFFICIAL GENE SYMBOL for the identifier, Gene list for the list type, and "Homo sapiens" for the protein species. Downloaded results encompassed "GOTERM_BP_DIRECT" for biological processes, "GOTERM_CC_DIRECT" for cellular components, "GOTERM_MF_DIRECT" for molecular functions, and "KEGG_PATHWAY" for pathway enrichment. From these findings, the top 10 GO terms and top 15 KEGG pathways, as determined by P-values, were

selected for highlighting in the presentation and elaboration of this study.

2.13. Molecular docking

The PDB Format of the top 5 target proteins by degree and the SDF format of the blood-incorporated constituents were collected in the Uniprot and PubChem databases for molecular docking via the CB-DOCK2 website (https://cadd.labshare.cn/cb-dock2/php/index.php) and save the molecular docking results.

2.14. Histological examination

Liver tissues that had been fixed for more than 24 h were removed from the fixative for trimming, dehydration, embedding, sectioning, HE staining and dehydration sealing, followed by microscopic examination and photographic analysis to assess morphological changes in each group.

2.15. Immunohistochemistry

Rat liver tissues previously fixed in 4 % paraformaldehyde fixative were removed and subjected to immunohistochemical experimental steps such as trimming, embedding, sectioning, staining and dehydration, followed by photographic analysis using Image-Pro Plus 6.0 to validate the five core targets closely associated with SSP anti-CH as screened by network pharmacology. Three 200 × fields of view were randomly selected for each section of rat liver tissue in each group to be photographed. The photographs were taken so that as much tissue as possible filled the entire field of view, and to ensure that the background light was as uniform as possible for each photograph. Image-Pro Plus 6.0 was used to select the same brown color as the standard for all positive

photographs, and each photograph was analyzed to obtain the cumulative optical density (IOD) and the pixel area of tissue (AREA) for each positive photograph.

3. Results

3.1. In vitro chemical composition identification

Under the above conditions, analysis of the methanolic extracts from SSP yielded the identification of 80 distinct chemical constituents. These included a diverse array of compounds: 17 alkaloids, 11 organic acids, 9 phenylpropanoids, 18 flavonoids, 8 terpenoids, 6 phenols, along with 11 other identified substances. To ensure the reliability of our findings, comparison with reference standards was performed, which confirmed the identity of 11 constituents within this profile. Visualization of the chemical composition was facilitated through both positive and negative ionization modes, which are comprehensively depicted in the mass flow diagrams presented in Fig. 2. Detailed characterizations of the principal chemical entities recognized in our analysis are collated and delineated in Table 1. This array of constituents underscores the complex phytochemical framework that SSP embodies, setting the stage for subsequent bioactivity correlations.

3.1.1. Alkaloids

Seventeen alkaloid compounds were identified from SSP. Several of these compounds, namely hordenine, protopine and coptisine were compared with the reference standards. For example, the compound dehydrocorydaline (Rt = 15.12 min, $C_{22}H_{23}NO_4$), gives a quasi-ion peak which is m/z 366.17029[M + H]$^+$. It loses one molecule of CH3 and one molecule of CO to form fragment ions m/z 351.14609 [M−CH$_3$]$^+$ and m/z 308.12805 [M−CH$_3$−CH$_3$−CO]$^+$ respectively (Guan et al., 2017) (Fig. 3A).
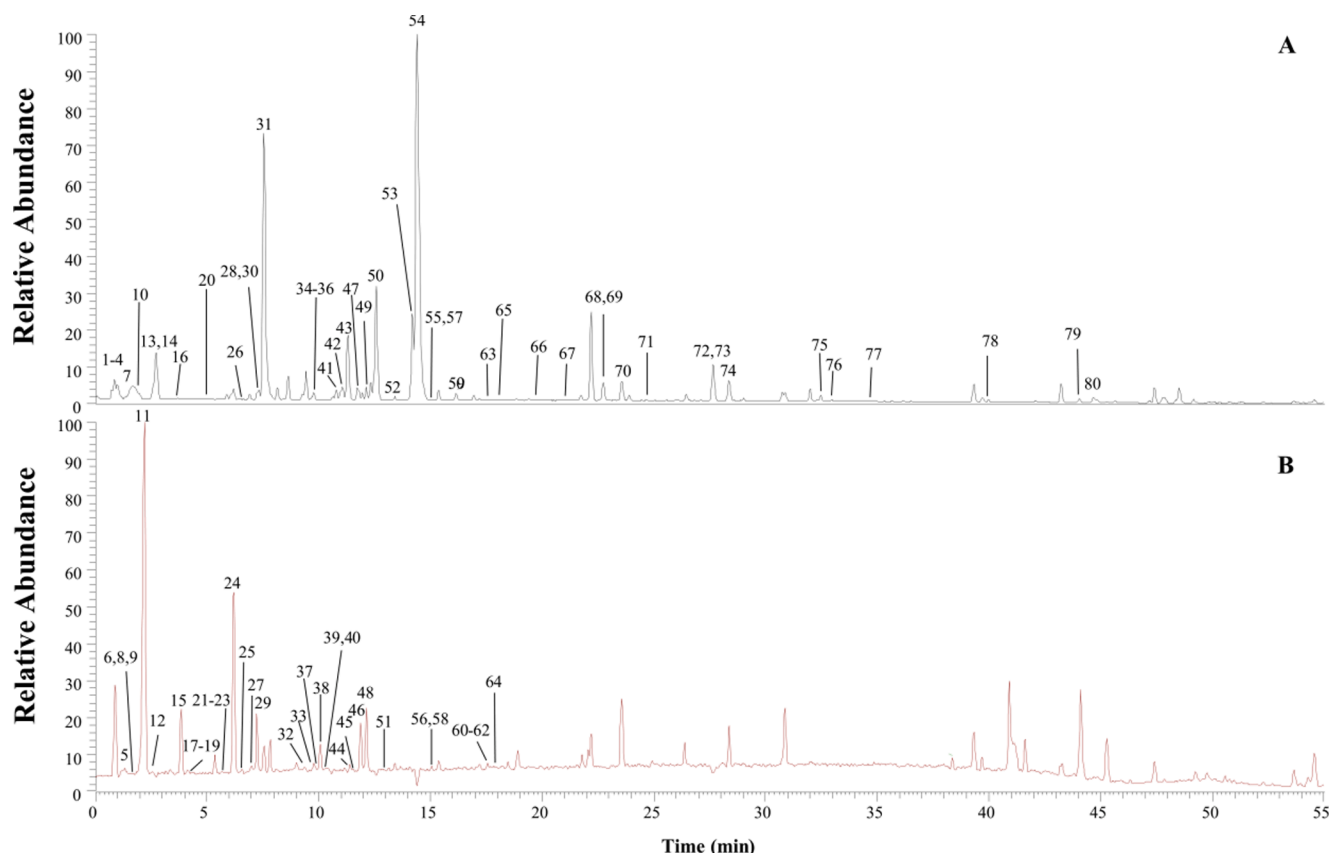

Fig. 2. Total ion flow diagram in the positive **(A)** and negative **(B)** ion modes of SSP.

Table 1

Information on chemical constituents identified from SSP.

NO.	t_R/min	Molecular formula	Precursor ion	Measured ion	Ion type	MS/MS(m/z)	Component	Classification
1	0.87	$C_5H_{13}NO$	103.10010	103.10015	$[M + H]^+$	104.10733,58.06580,60.08146	Choline(Bruce et al., 2010, Gill et al., 2020)	B
2	0.91	$C_7H_7NO_2$	137.04770	137.04772	$[M + H]^+$	138.05504,94.06558,92.05013	Trigonelline(Lang et al., 2008)	A
3	1.02	$C_5H_7NO_3$	129.04300	129.04297	$[M + H]^+$	130.05000,102.05524,84.04494,77.63916	Pyroglutamic acid(Qu et al., 2002)	G
4*	1.10	$C_{10}H_{15}NO$	165.11550	165.11551	$[M + H]^+$	166.12263,121.06499,103.05468	Hordenine(Steiner et al., 2016)	A
5	1.29	$C_7H_{10}O_5$	174.05226	174.05226	$[M-H]^-$	173.04494,129.01848,111.00776	Shikimic acid (Li et al., 2021)	B
6	1.30	$C_4H_6O_5$	134.02070	134.02069	$[M-H]^-$	133.01337,115.00274,71.01277	Malic acid (Birkler et al., 2010)	B
7	1.36	$C_4H_4N_2O_2$	112.02770	112.02771	$[M + H]^+$	113.03482,96.00844,70.02937	Uracil (Tafzi et al., 2020)	G
8	1.48	$C_6H_6O_6$	174.01590	174.01591	$[M-H]^-$	173.08185,137.02399,111.00781, 93.03360,85.02845,73.02847	Cis-Aconitic acid (Xiong et al., 2021)	B
9	1.58	$C_4H_6O_4$	118.02570	118.02575	$[M-H]^-$	117.05405,116.92759,99.02480,73.02842	Succinic acid (Yang et al., 2016)	B
10*	2.01	$C_{10}H_{15}NO$	165.11550	165.11551	$[M + H]^+$	166.12270,121.06500,103.05466	Hordenine(Steiner et al., 2016)	A
11*	2.19	$C_7H_6O_5$	170.02090	170.02091	$[M-H]^-$	169.01353,125.02351,124.01560,97.02856, 81.03366,79.01788,69.03351	Gallic acid (Huang et al., 2017, Ren et al., 2021)	B
12	2.19	$C_6H_6O_3$	126.03080	126.03079	$[M-H]-$	125.02354,97.02837,81.03336,61.39196	Pyrogallol (Dutschke et al., 2021)	F
13	2.75	$C_{12}H_{16}N_2O$	204.12630	204.12631	$[M + H]^+$	205.13388,160.07574,142.06523,132.08086, 115.05460,79.79268,67.02159,58.06585	Bufotenin (Costa et al., 2005)	A
14	2.88	$C_6H_6O_3$	126.03200	126.03202	$[M + H-H_2O]^+$	109.02871,81.03405,53.03931	5-Hydroxymethylfurfural (Zhou and Qi, 2017)	G
15	3.85	$C_7H_6O_4$	154.02590	154.02589	$[M-H]^-$	153.01851,109.02852	2,3-Dihydroxybenzoic (Cheiran et al., 2019)	B
16	3.86	$C_6H_6O_3$	126.03200	126.03199	$[M + H]^+$	127.03914,97.02858,71.04969,55.01853	Maltol (Li et al., 2011a; Zhang et al., 2002)	G
17	4.13	$C_{16}H_{24}O_{10}$	376.13701	376.13701	$[M-H]^-$	375.12570,213.07629,195.06602,169.08629, 161.04520,151.07524	8-epi-loganic acid (Wang, 2021)	E
18	4.29	$C_{16}H_{18}O_9$	354.09540	354.09535	$[M-H]^-$	353.08743,191.05566,179.03435,173.04437, 135.04431	Neochlorogenic acid (Fang et al., 2002)	C
19	4.32	$C_{16}H_{24}O_{10}$	376.13700	376.13698	$[M-H]^-$	376.13339,375.12900,213.07639,179.03410, 169.08633,125.05962,113.02348	Loganic acid (Zhou et al., 2021, Abirami et al., 2022)	E
20	4.89	$C_{12}H_{12}N_2O$	200.09510	200.09513	$[M + H]^+$	201.10213,186.07864,160.07579,114.94859, 81.07304	Harmalol (Zhang et al., 2013)	F
21	5.74	$C_8H_8O_5$	184.03660	184.03663	$[M-H]^-$	183.02925,140.01064,124.01566	Methyl gallate (Gong et al., 2020)	F
22	5.75	$C_7H_6O_4$	154.02590	154.02588	$[M-H]^-$	153.01851,123.00783,109.02851,108.02068	Gentisic acid (Yao et al., 2020)	F
23	5.90	$C_{16}H_{18}O_9$	354.09520	354.09518	$[M-H]^-$	353.08875,191.05548,161.02380	Chlorogenic acid (Zhang et al., 2010, Choi et al., 2018)	C
24*	6.15	$C_{16}H_{22}O_{10}$	420.12660	420.12663	$[M + HCOOH-H]^-$	419.11935,179.05539,161.04469,141.01843	Swertiamarin (Li et al., 2011b)	E
25	6.58	$C_9H_6O_4$	178.02630	178.02628	$[M-H]^-$	179.02368,178.05304,175.96822,177.01865, 176.83632,133.02861,121.02853,116.92731,105.03364	Esculetin (Yang et al., 2017)	C
26	6.58	$C_{16}H_{17}NO_3$	271.12090	271.12093	$[M + H]^+$	272.12808,255.10139,237.09093,209.09583,161.05962, 143.04916,123.04419,107.04949	Higenamine (Wang et al., 2020)	A
27	6.92	$C_7H_6O_4$	154.02590	154.02588	$[M-H]^-$	153.01846,152.89421,109.02850,108.02081	Protocatechuic acid (Li et al., 2017)	F
28*	7.22	$C_{19}H_{18}O_{11}$	422.08491	422.08491	$[M + H]^+$	423.09219,405.08167,359.13364,303.04977,167.01286	Mangiferin (Khurana et al., 2017)	D
29	7.23	$C_{19}H_{18}O_{11}$	422.08480	422.08482	$[M-H]^-$	421.07764,331.04593,301.03531	Isomangiferin (Aabideen et al., 2020)	D
30	7.26	$C_{16}H_{22}O_9$	358.12650	358.12645	$[M + H]^+$	359.13373,197.08073,179.07018,127.03906	Sweroside (Sheng et al., 2014)	E
31	7.54	$C_{20}H_{23}NO_4$	341.16300	341.16292	$[M + H]^+$	342.16986,297.11203,282.08856,265.08585,237.09108	Magnoflorine (Sharma et al., 2020; Tian et al., 2014a)	A
32	9.32	$C_{34}H_{28}O_{22}$	788.10790	788.10791	$[M-H]^-$	787.09906,617.07733,465.06805,447.05438,313.05780, 169.01355	1,2,3,6-Tetra-O-galloyl-β-D-glucose(Owen et al., 2003)	G
33	9.60	$C_{29}H_{36}O_{16}$	640.20040	640.20044	$[M-H]^-$	639.19299,477.16125,179.03438,161.02367,133.02861	Plantamajoside (Bai et al., 2017)	C
34	9.61	$C_{15}H_{16}O_8$	324.08460	324.08461	$[M + H]^+$	325.09180,163.03894,135.04411	Skimmin (Lou et al., 2020)	C
35*	9.62	$C_{10}H_8O_4$	192.04240	192.04237	$[M + H]^+$	193.04951,178.02605,165.05479,150.03110,137.05975, 133.02844,122.03632,105.07030,94.04187	Scopoletin (LI et al., 2022b; Wang et al., 2021; Zeng et al., 2015)	C
36	9.78	$C_{10}H_{10}O_4$	194.05800	194.05802	$[M + H]^+$	195.08740,193.15872,149.05971,145.02841,117.03373	Ferulic acid (Huang et al., 2014; Zhang et al., 2018b)	B
37	9.87	$C_{27}H_{30}O_{16}$	610.15360	610.15363	$[M-H]^-$	609.14600,343.04520,300.02744,271.02481,151.00293	Rutin (He et al., 2014)	D
38*	10.07	$C_{14}H_6O_8$	302.00630	302.00625	$[M-H]^-$	300.99884,283.99612,257.00876,229.01373,185.02370	Ellagic acid (Yan et al., 2014)	F
39	10.32	$C_{21}H_{20}O_{12}$	464.09580	464.09580	$[M-H]^-$	463.08807,300.02753,271.02475,151.00276	Isoquercitrin (Zhang et al., 2017)	D
40	10.36	$C_{29}H_{36}O_{15}$	624.20570	624.20570	$[M-H]^-$	623.19843,461.16479,315.10901,179.03447,161.02365, 135.04425,133.02858,113.02342	Verbascoside (Plaza et al., 2005, Wu et al., 2006, Xie et al., 2017)	F
41	10.78	$C_{21}H_{25}NO_4$	355.17840	355.17836	$[M + H]^+$	356.18555,192.10184,177.07835	Tetrahydropalmatine (Wang et al., 2019)	A

(*continued on next page*)

Table 1 (*continued*)

NO.	t_R/min	Molecular formula	Precursor ion	Measured ion	Ion type	MS/MS(m/z)	Component	Classification
42	10.96	$C_{27}H_{30}O_{15}$	594.15860	594.15863	$[M+H]^+$	595.16595,593.15143,285.04044,284.03268,255.02959	Kaempferol-3-O-rutinoside (Dou et al., 2017; Li et al., 2020a)	D
43*	11.30	$C_{20}H_{19}NO_5$	353.12640	353.12639	$[M+H]^+$	354.13342,189.07861,188.07057,149.05974	Protopine (Huang et al., 2014)	A
44	11.32	$C_{25}H_{24}O_{12}$	516.12680	516.12680	$[M–H]^-$	517.12518,515.11249,353.08768,173.04465,161.02365	4,5-Dicaffeoylquinic (de Souza et al., 2015, Pantoja Pulido et al., 2017)	C
45	11.57	$C_{21}H_{20}O_{11}$	448.10070	448.10070	$[M–H]^-$	447.09299,301.03516,300.02747,284.03229	Kaempferol-3-glucoside (Abu Bakar et al., 2020)	D
46	11.66	$C_9H_8O_3$	164.0469	164.0469	$[M–H]^-$	163.03943,119.04929	p-Coumaric acid (Yao et al., 2017)	B
47	11.73	$C_{21}H_{20}O_{10}$	432.10580	432.10577	$[M+H]^+$	431.09805,268.03778,269.04593	Apigetrin (Yilmaz et al., 2018)	D
48	12.08	$C_{25}H_{24}O_{12}$	516.12670	516.12666	$[M–H]^-$	515.04901,353.08768,191.05547,179.03429, 173.04483,135.04422	Isochlorogenic acid C(Huang et al., 2015)	C
49	12.11	$C_{21}H_{23}NO_5$	369.15760	369.15861	$[M+H]^+$	370.16479,352.15436,336.12405,290.09338, 206.08112,189.07838,188.07063,165.09113	Allocryptopine (Huang et al., 2018)	A
50	12.57	$C_{20}H_{19}NO_4$	305.10530	305.10527	$[M+H+MeOH]^+$	338.13846,322.10745,279.08893,265.07349	Jatrorrhizine (Li et al., 2019)	A
51	12.93	$C_{21}H_{20}O_{10}$	432.10580	432.10581	$[M–H]^-$	431.09824,284.03259,151.00270,107.01329	Afzelin (Abu Bakar et al., 2020, Brito et al., 2021)	D
52	13.40	$C_{29}H_{30}O_{13}$	586.16870	586.16873	$[M+H]^+$	587.17621,391.10229,373.09274,311.09113, 281.08109,247.05984,197.08087	Amarogentin (Kumar and Chandra, 2015)	E
53	13.92	$C_{20}H_{13}NO_4$	331.08450	331.08446	$[M+H]^+$	332.09143,317.06812,274.08600,246.09132, 218.09642	Sanguinarine (Xie et al., 2015)	A
54*	14.39	$C_{19}H_{14}NO_4$	320.0909	320.09146	$[M+H]^+$	321.09821,292.09665,290.08130,262.08636, 249.07773,234.09081	Coptisine (Cheng et al., 2016)	A
55	15.06	$C_{16}H_{12}O_5$	284.06850	284.06854	$[M+H]^+$	285.07553,270.05209,253.04935,225.05449,214.06219, 213.05453,137.02330	Calycosin (Sun et al., 2014)	D
56	15.06	$C_{15}H_{10}O_6$	286.04780	286.04777	$[M–H]^-$	285.04034,270.04449,257.04575,241.05025,217.05042, 201.01904,199.03970,198.03168,175.03946,171.04475, 151.00288,133.02859,132.02080,121.02863,107.01289	Luteolin (Xie et al., 2017, Jia et al., 2020, Meng et al., 2020)	D
57	15.12	$C_{22}H_{23}NO_4$	365.16310	365.16313	$[M+H]^+$	366.16989,351.14609,350.13846,322.14340,308.12805, 306.11206,278.52924	Dehydrocorydaline (Guan et al., 2017)	A
58*	15.14	$C_{15}H_{10}O_7$	302.04270	302.04269	$[M–H]^-$	301.03522,178.99797,151.00284	Quercetin (Zhang et al., 2018a)	D
59	16.15	$C_{20}H_{17}NO_4$	335.11600	335.11604	$[M+H]^+$	336.12286,320.09164,292.09647,278.08099	Berberine (Xu et al., 2015)	A
60	17.49	$C_{16}H_{12}O_6$	300.06340	300.06340	$[M–H]^-$	299.05588,284.03250,136.98711,65.00219	Diosmetin (Shi et al., 2018)	D
61	17.51	$C_{26}H_{45}NO_7S$	515.29160	515.29163	$[M–H]^-$	51428412,124.00652,106.97980,80.96410	Taurocholic acid (Gu et al., 2016)	G
62	17.57	$C_{13}H_8O_6$	260.03200	260.03198	$[M–H]^-$	259.02463,231.02921,215.03450,203.03465,187.03944, 151.00305	Tetrahydroxyxanthone (Guo et al., 2018)	D
63	17.57	$C_{15}H_{10}O_3$	238.06310	238.06307	$[M+H]^+$	239.06999,221.05798,165.06998,133.08617,121.02856 ,93.03368,65.03925	3-Hydroxyflavone (Xu et al., 2013)	D
64	17.91	$C_{18}H_{18}O_4$	298.12060	298.12062	$[M–H]^-$	297.11307,189.05511,93.03343	Enterolactone (Parker et al., 2012)	G
65	17.99	$C_{17}H_{14}O_7$	330.07400	330.07403	$[M+H]^+$	331.08096,316.05759,301.03369,168.00523	Jaceosidin (Song et al., 2009)	D
66	19.64	$C_{21}H_{24}O_6$	372.15740	372.15736	$[M+H]^+$	373.16293,355.15359,337.14331,323.12579,305.11682, 295.13278,237.11182,177.05486,165.05507,151.07533, 137.05975,121.06496	Arctigenin (Zou et al., 2013)	C
67	21.09	$C_{17}H_{14}O_7$	330.07410	330.07410	$[M+H]^+$	331.08130,329.06671,314.04315,299.01971,271.02496	Iristectorigenin B (Mykhailenko et al., 2020)	D
68	22.51	$C_{16}H_{12}O_5$	284.06850	284.06855	$[M+H]^+$	285.07568,270.05209,242.05725,170.11955	5,7-Dihydroxy-4′-methoxyisoflavone (Beszterda et al., 2020)	D
69	22.96	$C_{14}H_{10}O_6$	274.04785	274.04785	$[M+H]^+$	275.04572,273.04037;258.01682;230.02197; 186.03223	Bellidifolin (Wang et al., 2015)	D
70	23.43	$C_{17}H_{21}NO_3$	287.15220	287.15218	$[M+H]^+$	289.16284,288.15927,175.07491,161.05911, 135.04410,86.09696,84.08147	Piperanine (Friedman et al., 2008)	A
71	24.63	$C_{17}H_{19}NO_3$	285.13650	285.13649	$[M+H]^+$	286.14377,285.13556,215.10611,201.05458, 171.04402,143.04916,135.04413,112.07600, 98.06050,84.08131,69.07053	Piperine (Chithra et al., 2014)	A
72*	27.66	$C_{15}H_{20}O_2$	232.14658	232.14658	$[M+H]^+$	233.15387,187.14812,159.11681,145.10123, 131.08563	Costunolide (Pei et al., 2012)	E
73	28.00	$C_{15}H_{20}O_2$	232.14660	232.14659	$[M+H]^+$	233.15367,215.14308,187.14815,105.07028	Isoalantolactone (Kumar et al., 2014)	E
74*	28.37	$C_{15}H_{18}O_2$	230.13080	230.13083	$[M+H]^+$	231.13792,213.12744,195.11662,185.13248, 175.07539,157.10126,143.08556	Dehydrocostus lactone (Kumar et al., 2014)	E
75	32.71	$C_{20}H_{15}NO_4$	333.09980	333.09981	$[M+H]^+$	334.10687,319.08377,276.10138	Dihydrosanguinarine (Xie et al., 2015)	A

Table 1 (continued)

NO.	t_R/min	Molecular formula	Precursor ion	Measured ion	Ion type	MS/MS(m/z)	Component	Classification
76	32.97	$C_{18}H_{30}O_3$	294.21950	294.21963	[M + H-H$_2$O]$^+$	277.21631,249.22151,185.113248,125.09607	9-Oxo-10(E),12(E)-octadecadienoic (Kim et al., 2011)	B
77	34.65	$C_{20}H_{37}NO_2$	323.28260	323.28261	[M + H]$^+$	324.28934,306.52356,109.10160,95.08610, 62.06074	Linoleoyl ethanolamide (Palandra et al, 2009)	G
78	39.99	$C_{18}H_{35}NO$	281.27200	281.27198	[M + H]$^+$	282.27927,247.24199,57.07064	Oleamide (Farha and Hatha, 2019)	G
79	44.07	$C_{22}H_{43}NO$	337.33450	337.33449	[M + H]$^+$	338.34155,321.31519,303.30380,163.14795, 149.13245,135.11687,111.11709	Erucamide (Dabur and Mittal, 2016)	G
80	44.68	$C_{18}H_{37}NO$	283.28760	283.28755	[M + H]$^+$	284.29474,116.10712,102.09167,71.04993, 57.07061	Stearamide (Castillo-Peinado et al., 2019)	G

Note: A, Alkaloids; B, Organic acids; C, Phenylpropanoids; D, Flavonoids; E, Terpenoids; F, Phenols; G, Others respectively. "*" is the ingredient confirmed by comparing with the reference substance.

3.1.2. Organic acids

Eleven organic acids were identified from SSP, including gallic acid, which was accurately identified by comparison with the reference standards. For example, the compound gallic acid (Rt = 2.19 min, $C_7H_6O_5$), gives a quasi-ion peak which is m/z 169.0136[M-H]$^-$. It loses a COOH molecule to form the fragment ion m/z 124.01560 [M−H−COOH]$^-$. It breaks its C–C bond f to form m/z 125.02351 [M−H−CO$_2$]$^-$ and m/z 97.02856 [M−H−CO$_2$−CO]$^-$, respectively, and loses another H$_2$O molecule to form the fragment ion m/z 79.01788 [M−H−CO$_2$−CO−H$_2$O]$^-$ (Huang et al., 2017, Ren et al., 2021) (Fig. 3**B**).

3.1.3. Phenylpropanoids

Nine phenylpropanoids were identified from SSP, among which scopoletin was accurately identified by comparing with the reference standards. For example, scopoletin (Rt = 9.62 min, $C_{10}H_8O_4$), gives a quasi-ion peak which m/z is 193.04971[M + H]$^+$. The C-O bond on the side chain of the benzene ring breaks to form fragment ions with m/z 178.02605 [M + H-CH$_3$]$^+$. The benzene ring break formed m/z 165.05479 [M + H-CO]$^+$ and the carbon chain continued to break to form m/z 137.05975 [M + H-2CO]$^+$ (LI et al., 2022b; Wang et al., 2021; Zeng et al., 2015) (Fig. 3**C**).

3.1.4. Flavonoids

Eighteen flavonoids were identified from SSP, among which mangiferin and quercetin was accurately identified by comparing with the reference standards. For example, luteolin (Rt = 15.06 min, $C_{15}H_{10}O_6$), obtained a quasi-ion peak which m/z is 285.04047[M-H]$^-$. The C-O bond is broken to form m/z 270.04449 [M−H−O]$^-$. After RDA cleavage, m/z 151.00288 and m/z 133.02859 were formed (Xie et al., 2017, Jia et al., 2020, Meng et al., 2020) (Fig. 3**D**).

3.1.5. Terpenoids

Eight terpenoids were identified from SSP, among which swertiamarin, costunolide and dehydrocostus lactone were accurately identified by comparison with the reference standards. Sweroside (Rt = 7.26 min, $C_{16}H_{22}O_9$), the quasi-ion peak m/z 359.13373 [M + H]$^+$ was obtained. The formation of fragment ions after the glycosidic bond is visible in the secondary mass spectrum m/z 197.08073 and m/z 179.05539 (Yu, 2017) (Fig. 3**E**).

3.1.6. Phenolics

Six phenolic compounds were identified from SSP, of which ellagic acid was accurately identified by comparison with the reference standards. For example, verbascoside (Rt = 10.36 min, $C_{29}H_{36}O_{15}$), obtained a quasi-ion peak m/z 623.19843[M-H]$^-$. The glycosidic bond was broken to form m/z 179.03447 and m/z 161.02365, and the loss of a further CO molecule resulted in the formation of m/z 135.04425 (Plaza et al., 2005, Wu et al., 2006, Xie et al., 2017) (Fig. 3**F**).

3.1.7. Others

Eleven other compounds were identified from SSP. For example, stearamide (Rt = 44.68 min, $C_{18}H_{37}NO$), obtained a quasi-ion peak of m/z 284.29483 [M + H]$^+$. C–C bond breakage forms m/z 71.04993 and m/z 57.07061(Castillo-Peinado et al., 2019) (Fig. 3**G**).

3.2. In vivo chemical composition identification

The plasma samples of rats in the dosing and blank groups were analyzed and identified according to the above conditions. The results obtained from the 10-fold dosing group were discarded as they were fewer. A total of 20 chemical components, including 10 prototypes and 10 metabolites, were detected and analyzed in plasma samples from the 20-fold dosing group, net of the chemical components of the blank group. The total positive and negative ion flow diagrams of the samples are shown in Fig. 4, the results of the identification of the main

components are shown in Table 2 and the structural formulae of the main components are shown in Fig. 5.

3.2.1. Prototype composition identification

A total of ten prototype components were identified from the plasma of rats given SSP by gavage, including gallic acid, methyl gallate, swertiamarin, mangiferin, isomangiferin, ellagic acid, taurocholic acid, bellidifolin, oleamide and erucamide.

Gallic acid (Rt = 2.27 min, $C_7H_6O_5$), a quasi-ion peak of m/z 169.0136 [M−H]$^-$ was obtained. Loss of one carbon dioxide and one carbon monoxide resulted in the formation of m/z 125.02351 [M−H−CO$_2$]$^-$ and m/z 97.02839 [M−H−CO$_2$−CO]$^-$, respectively. Loss of two carbon dioxide forms m/z 69.03351 [M−H−CO$_2$−2CO]$^-$ (Huang et al., 2017, Ren et al., 2021) (Fig. 6**A**).

Swertiamarin (Rt = 6.21 min, $C_{16}H_{22}O_{10}$), a quasi-ion peak of m/z 419.11975 [M + HCOOH-H]$^-$ was obtained. Its glycosidic bond is broken to form m/z 179.05331 (Li et al., 2011b) (Fig. 6**B**).

Ellagic acid (Rt = 10.05 min, $C_{14}H_6O_8$), obtained a quasi-ion peak of m/z 300.99899 [M−H]$^-$. The parent ion loses one OH molecule to form m/z 283.99622 [M−H−OH]$^-$; one HCOOH molecule and one CO molecule to form m/z 229.01414 [M−H−CO$_2$−CO]$^-$, and another CO$_2$ molecule to form m/z 185.02397 [M−H−2CO$_2$−CO]$^-$ (Yan et al., 2014, Qin et al., 2016) (Fig. 6**C**).

3.2.2. Metabolite identification

A total of 10 metabolic components, including valine, leucine, 3-hydroxybutyric acid, caprolactam, 6-acetylmorphine, hydrastine, indole-3-acetic acid, p-nitrophenol, palmitoleic acid and naringenin, were identified in the plasma of rats given SSP by gavage.

Naringenin (Rt = 16.98 min, $C_{15}H_{12}O_5$), obtained a quasi-ion peak of m/z 271.06140 [M−H]$^-$. The chemical bond on the C ring is broken to form m/z 177.01878 [M−H−C$_5$H$_2$O$_2$]$^-$ and m/z 151.00288 [M−H−C$_8$H$_8$O]$^-$. A CO$_2$ is removed from m/z 151.00288 [M−H−C$_8$H$_8$O]$^-$ to form m/z 107.01286 [M−H−C$_9$H$_8$O3]$^-$ (Sun et al., 2020) (Fig. 6**D**).

Hydrastine (Rt = 9.63 min, $C_{21}H_{21}NO_6$), obtained a quasi-ion peak of m/z 384.14429 [M + H]$^+$. The fragment ion m/z 190.08638 [M + H-C$_{10}$H$_9$O$_4$]$^+$ is seen in the secondary mass spectrum after a chemical bond breakage (Gupta et al., 2015) (Fig. 6**E**).

3.3. Network pharmacological analysis of 20 blood-incorporated constituents

3.3.1. The targets of SSP blood-incorporated constituents and CH

Employing the SwissTargetPrediction database, our study identified 467 potential targets associated with the blood-incorporated constituents of SSP. These were cross-referenced with a set of 916 targets implicated in CH pathophysiology. This comparative analysis culminated in a subset of 103 common targets, presenting a focused pool of candidates that may mediate SSP's anti-CH effects (Fig. 7**A**).

3.3.2. Protein-protein interaction (PPI) network construction

To elucidate the potential interactions among the 103 overlapping targets identified, we established a PPI network comprising these targets. The network consisted of 103 nodes representing targets and 779 edges denoting interactions, with a median connectivity degree of 15.1, illustrating a complex web of potential inter-target communications (Fig. 7**B**). Analysis of this PPI network highlighted the top 10 core targets with the highest degree values, namely AKT, VEGFA, CASP3, SRC, MAPK3, ESR1, MMP9, PTGS2, PPARG, and MAPK8, indicating their centrality within the network and their possible significance in SSP's anti-CH action (Fig. 7**C**). To further explore the relationships between the blood-incorporated constituents of SSP and the intersecting targets, we constructed an interaction network graph. This graphical representation allowed us to discern that, of the 20 components analyzed, three exhibited no direct targets. Conversely, palmitoleic acid, naringenin,

and hydrastine emerged as the three constituents with the widest scope of target interactions, hinting at their prominent roles within the therapeutic context of SSP against CH (Fig. 7**D**).

3.3.3. GO and KEGG pathway enrichment analysis

To delineate the underlying mechanisms of SSP's therapeutic effect on CH, we input the 103 overlapping targets into the DAVID database for GO and KEGG pathway analyses. The GO functional enrichment analysis identified significant associations with 394 biological processes (BP), with top-ranking processes by P-value encompassing responses to drugs, negative regulation of apoptosis, and intracellular receptor signaling pathways. Within cellular components (CC), 56 entities were implicated, with notable structures including receptor complexes, membrane rafts, and the plasma membrane. For molecular functions (MF), 107 functions were highlighted, with steroid binding, enzyme binding, and zinc ion binding surfacing as impactful (Fig. 8**A**).

KEGG pathway enrichment analysis disclosed 142 pathways potentially pertinent to SSP's pharmacodynamics, from which the top 15 pathways were selected based on enrichment significance (Fig. 8**B**). Some pathways corresponding to the blood-incorporated constituents of SSP stood out, like AGE-RAGE signaling associated with diabetic complications, apoptosis, TNF signaling pathway, and VEGF signaling pathways, etc. Noteworthy pathways not displayed in the top selection included the Rap1 signaling pathway (P = 9.78E-07), fluid shear stress and atherosclerosis (P = 5.05E-06), and the sphingolipid signaling pathway (P = 1.03E-05). Excitingly, we found that top 5 core targets were the most enriched in the VEGF signaling pathway. Therefore, VEGF is considered to be the key pathway for SSP to play its role in the treatment of CH (Fig. 8**C**).

3.3.4. Molecular docking

Based on the PPI network and pathway enrichment results, we performed molecular docking of the top 5 target proteins in terms of degree (most of which were also significantly enriched in the VEGF signalling pathway) and the 17 blood-incorporated constituents associated with CH, and the detailed results of molecular docking are shown in Fig. 9**A**. Of all the chemical-target combinations examined, the three pairs exhibiting the lowest binding energies, indicative of the strongest predicted interactions, were: ellagic acid with MAPK3 (Fig. 9**B**), ellagic acid with VEGFA (Fig. 9**C**), and hydrastine with SRC (Fig. 9**D**). In addition to these findings, the docking scores involving six constituents (including swertiamarin, 6-acetylmorphine, hydrastine, ellagic acid, taurocholic acid, and bellidifolin) in relation to the five core targets were uniformly below −6 kcal/mol, underscoring the potential strength and significance of their interactions. It is noteworthy that swertiamarin, ellagic acid, taurocholic acid, and bellidifolin were discerned as prototype components, being those most reliably detected in the bloodstream post SSP administration. These analyses collectively suggest that these four constituents may play an integral role in mediating SSP's therapeutic efficacy against CH, signifying the potential for their advancement as focal points for further study and drug development efforts against this condition.

3.3.5. Biological validation

To evaluate the therapeutic potential of SSP for combating CH, our study commenced with histological investigation through H&E staining. In normal control rats, hepatocytes demonstrated a radiating arrangement around central veins, exhibiting typical morphology and intact architecture without prominent histopathological deviations. In contrast, rats from the model control group, depicting a similar radial hepatocyte organization, exhibited discernible pathologic alterations, including hepatocyte vacuolation, infiltration of inflammatory cells within confluent regions, necrotic sites within hepatic tissues accompanied by local congestive or hemorrhagic features. Upon treatment with SSP, we observed a restoration towards normalcy in the arrangement of hepatocytes around central veins across various dosage groups.
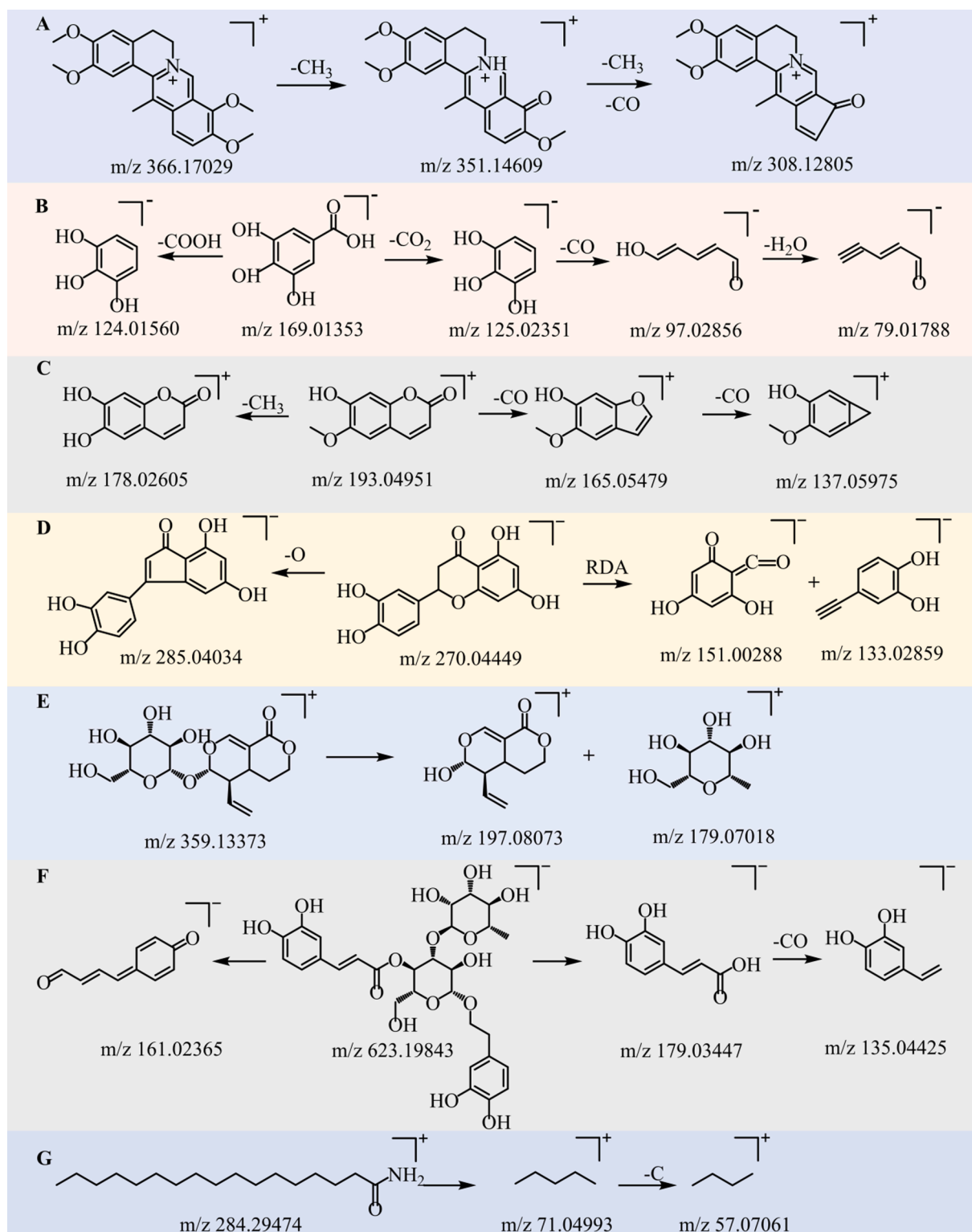
Fig. 3. The possible fragmentation pathways of the major components identified from SSP. **(A)** Dehydrocorydaline. **(B)** Gallic acid. **(C)** Scopoletin. **(D)** Luteolin. **(E)** Sweroside. **(F)** Verbascoside. **(G)** Stearamide.

There was noticeable amelioration in steatotic vacuolization and reduced inflammatory exudation (Fig. 10A). Based on the results of network pharmacological analysis, we obtained that the top five core targets all have numerous studies showing that their aberrant expression or abnormally elevated activity may lead to different degrees of liver pathology, so we selected the top five proteins (AKT1, VEGFA, CASP3, SRC, MAPK3) that are closely related to the SSP anti-CH and verified the

targets using immunohistochemistry methods. Notably, most of these Top5 targets are enriched in the VEGF signalling pathway, thus, we examined the expression of these five target proteins using immuno-histochemistry, and the immunohistological quantifications revealed elevated expressions of AKT1, VEGFA, CASP3, SRC, and MAPK3 in the model group when compared to normal controls, with significant differences ($p < 0.001$). Compared with the model group, the UDCA, as

well as low, medium, and high doses of SSP, resulted in a dose-dependent attenuation in the expression levels of these proteins when juxtaposed against the model control. These alterations were statistically significant ($p < 0.05$) (Fig. 10B). These findings corroborate SSP's putative hepatoprotective effect and pave the way for a deeper understanding of SSP's mechanistic role.

4. Discussion

This research aimed to delineate the active chemical components and their mechanistic roles underpinning the therapeutic effects of the Tibetan medicine SSP in the management of CH. Through UHPLC-Q-Exactive Orbitrap/MS, we examined both the composition of SSP and the plasma constituents in SSP-dosed rats. We identified 80 chemical entities *in vitro* and 20 that were systemically assimilated, inclusive of 10 primary compounds and 10 derivative metabolites. Notables among these are gallic acid, swertiamarin, ellagic acid, and bellidifolin, each capable of targeting multiple biological sites. Gallic acid displays a spectrum of bioactivities, including anti-inflammatory, antiviral, and liver-protective effects (Huang et al., 2023). Specific to the liver, it targets and induces apoptosis in hepatic stellate cells and inhibits growth in the SMMC-7721 hepatocellular carcinoma cell line (Sun, 2016, Zheng et al., 2016). Swertiamarin has been reported to substantially abate both serum aspartate aminotransferase (AST) and interleukin-6 (IL-6) levels in models of surgically induced liver injury, and decrease serum alanine aminotransferase (ALT) and total bilirubin (TBIL) in chemical liver injury scenarios (Chen et al., 2016; Tian et al., 2014b; Zhang et al., 2015). Ellagic acid has been observed to reverse acute liver injury markers such as ALT and AST in mice, elevate the expression of VEGF and its receptor VEGFR, and boost CASP3 activity, underscoring its hepatoprotective capacity across both rodent species (Chen et al., 2023; Zhang et al., 2016b; Zhao et al., 2021; Long et al., 2017). Collectively, our findings affirm the medicinal significance of these compounds, ensuring their pivotal status in the exploration of SSP's mode of action in CH.

Network pharmacology analyses divulged 103 intersecting targets between components absorbed into the bloodstream following SSP administration and those implicated in CH, highlighting a spectrum of potential molecular sites for SSP's action against the disease. Subsequent establishment of a PPI network facilitated the distillation of five central targets of interest-AKT1, VEGFA, CASP3, SRC, and MAPK3-for therapeutic intervention. Kupffer cells (KCs) can instigate the synthesis and release of transforming growth factor-beta1 (TGF-β1), thereby contributing to hepatic inflammation, a response that is augmented in mice subjected to CCl$_4$-induced liver fibrosis mice (Ghavami et al., 2015, Nie et al., 2019, Vaidya et al., 2019). Research suggests that the inhibition of AKT1 may curtail TGF-β1 secretion by KCs, offering a therapeutic lever against liver inflammation (Wu et al., 2020). Meanwhile, VEGFA serves as a trigger for human hepatic stellate cell activation through VEGF-VEGFR pathways, whose attenuation has been documented to lessen the severity of NAFLD progression to hepatocellular carcinoma in mice with hepatocyte-specific VEGFA deletion (Vaidya et al., 2019). Overexpression of CASP3, with ensuing PARP substrate cleavage, precipitates DNA disintegration and cellular apoptosis-a common occurrence across various liver pathologies including inflammation, fibrosis, and cancer (Hengartner, 2000, Decker and Muller, 2002, Osna et al., 2017, Ma et al., 2021). Disparities in SRC expression are influential in liver functionality and bear prognostic significance in hepatocellular carcinoma trajectories (Chatzizacharias et al., 2012, Reinehr et al., 2013, Mantonakis et al., 2017). Additionally, aberrations in MAPK3′s expression or activity may instigate cellular apoptosis or proliferation, potentially influencing the onset, progression, or metastatic spread of diverse cancers, liver cancer included (Taherkhani et al., 2023). In the context of SSP's therapeutic targeting for CH, the elucidated PPI network underscores the five core targets (AKT1, VEGFA, CASP3, SRC, MAPK3) as vital nodes, potentially critical in the effective management of cholestatic hepatitis.

GO and KEGG pathway enrichment analyses were deployed to unravel the pharmacological mechanisms through which SSP counteract CH. According to GO insights, the implicated targets were
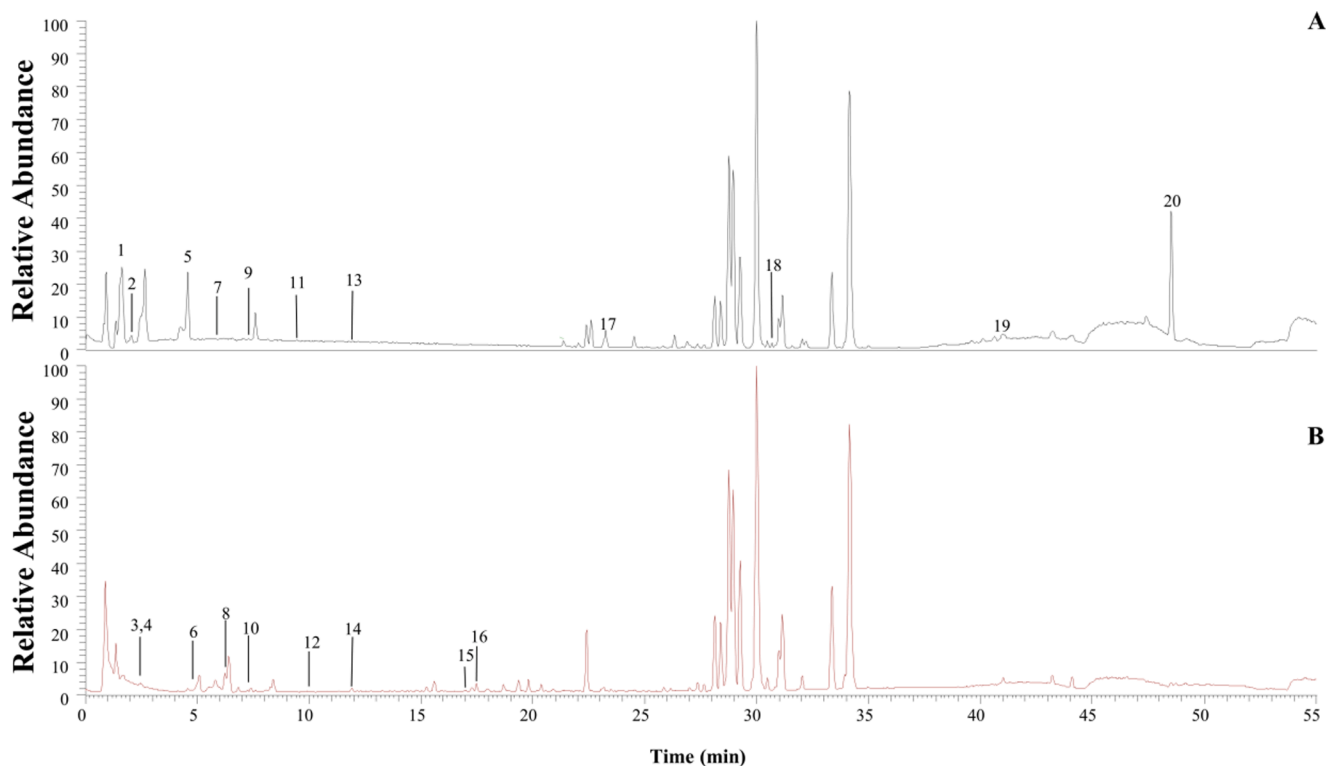

Fig. 4. The positive **(A)** and negative **(B)** ion chromatogram of the blood-incorporated constituents in SSP.

Table 2
Characterization of blood-incorporated constituents in SSP.

| NO.	t_R/min	Molecular formula	Precursor ion	Measured ion	Ion type	MS/MS (*m/z*)	Component	Classification
1	1.51	$C_5H_{11}NO_2$	117.07920	117.07923	[M + H]$^+$	118.08652,72.08141,55.05495	Valine(Virág et al., 2020)	Others
2	2.03	$C_6H_{13}NO_2$	131.09	131.09	[M + H]$^+$	132.10202;86.09697;69.07052;55.93526	Leucine (Xiong et al., 2021)	Others
3	2.27	$C_7H_6O_5$	170.02100	170.02096	[M−H]$^-$	169.01350,125.02351,124.88483,124.01545,97.02839,81.03327,69.03345	Gallic acid (Huang et al., 2017, Ren et al., 2021)	Organic acids
4	2.45	$C_4H_8O_3$	104.04650	104.04646	[M−H]$^-$	103.03909,59.01276	3-Hydroxybutyric (Zhang et al., 2016a)	Others
5	4.55	$C_6H_{11}NO$	113.08440	113.08438	[M + H]$^+$	114.09161,79.05477,55.01859,55.05495	Caprolactam (Wu et al., 2012)	Others
6	4.89	$C_8H_8O_5$	184.04	184.04	[M−H]$^-$	183.02948;140.01076;124.01572	Methyl gallate (Gong et al., 2020)	Organic acids
7	6.05	$C_{19}H_{21}NO_4$	327.14720	327.1472	[M + H]$^+$	328.15411,165.07037	6-Acetylmorphine (Ruiz-Colon et al., 2012)	Alkaloids
8	6.21	$C_{16}H_{22}O_{10}$	420.12700	420.12703	[M + HCOOH-H]$^-$	419.11975,179.05531,161.04503,141.01842	Swertiamarin (Li et al., 2011b)	Terpenoids
9	7.23	$C_{19}H_{18}O_{11}$	422.08491	422.08491	[M + H]$^+$	423.09116[M + H]$^+$,405.08170[M + H-H$_2$O]$^+$,387.07120,327.04993,303.04974[M + H-C$_4$H$_8$O$_4$]$^+$,273.03925[M + H-C$_4$H$_8$O$_4$-CH$_2$O]$^+$	Mangiferin (Khurana et al., 2017)	Flavonoids
10	7.25	$C_{19}H_{18}O_{11}$	422.08	422.09	[M−H]$^-$	421.0779;421.07712;331.04596;301.03531	Isomangiferin (Aabideen et al., 2020)	Flavonoids
11	9.63	$C_{21}H_{21}NO_6$	383.13700	383.13701	[M + H]$^+$	384.14429(32),190.08638	Hydrastine (Gupta et al., 2015)	Alkaloids
12	10.05	$C_{14}H_6O_8$	302.00640	302.00642	[M−H]$^-$	300.99899,283.99622,257.00824,229.01414,185.02397	Ellagic acid (Yan et al., 2014)	Phenols
13	11.97	$C_{10}H_9NO_2$	175.06350	175.06348	[M + H]$^+$	176.07048,130.06517,103.05463	Indole-3-acetic acid (Lin et al., 2015)	Others
14	12.10	$C_6H_5NO_3$	139.02620	139.02621	[M−H]$^-$	138.01881,108.02070,94.08684	4-Nitrophenol (Hernández et al., 2004)	Phenols
15	16.98	$C_{15}H_{12}O_5$	272.06860	272.06858	[M−H]$^-$	271.06116,227.07135,177.01878,165.01872,151.00288,119.04930,107.01286,93.03355,64.99896	Naringenin (Xu et al., 2020)	Flavonoids
16	17.48	$C_{26}H_{45}NO_7S$	515.29190	515.29187	[M−H]$^-$	514.28442,124.00647,106.97991,80.96426	Taurocholic acid (Gu et al., 2016)	Others
17	23.50	$C_{14}H_{10}O_6$	274.05	274.05	[M + H]$^+$	275.05505;273.04041;258.01697;230.02174;186.03177	Bellidifolin (Wang et al., 2015)	Flavonoids
18	30.69	$C_{16}H_{30}O_2$	254.22	254.22	[M + H]$^+$	255.23184;237.22174;95.08604	Palmitoleic acid (Luo et al., 2022)	Others
19	40.91	$C_{18}H_{35}NO$	281.27170	281.27165	[M + H]$^+$	282.27896,114.09157,57.07048	Oleamide (Farha and Hatha, 2019)	Others
20	48.52	$C_{22}H_{43}NO$	337.33450	337.33455	[M + H]$^+$	338.34152,321.31485,303.30420,163.14018,149.13278,135.11661	Erucamide (Dabur and Mittal, 2016)	Others
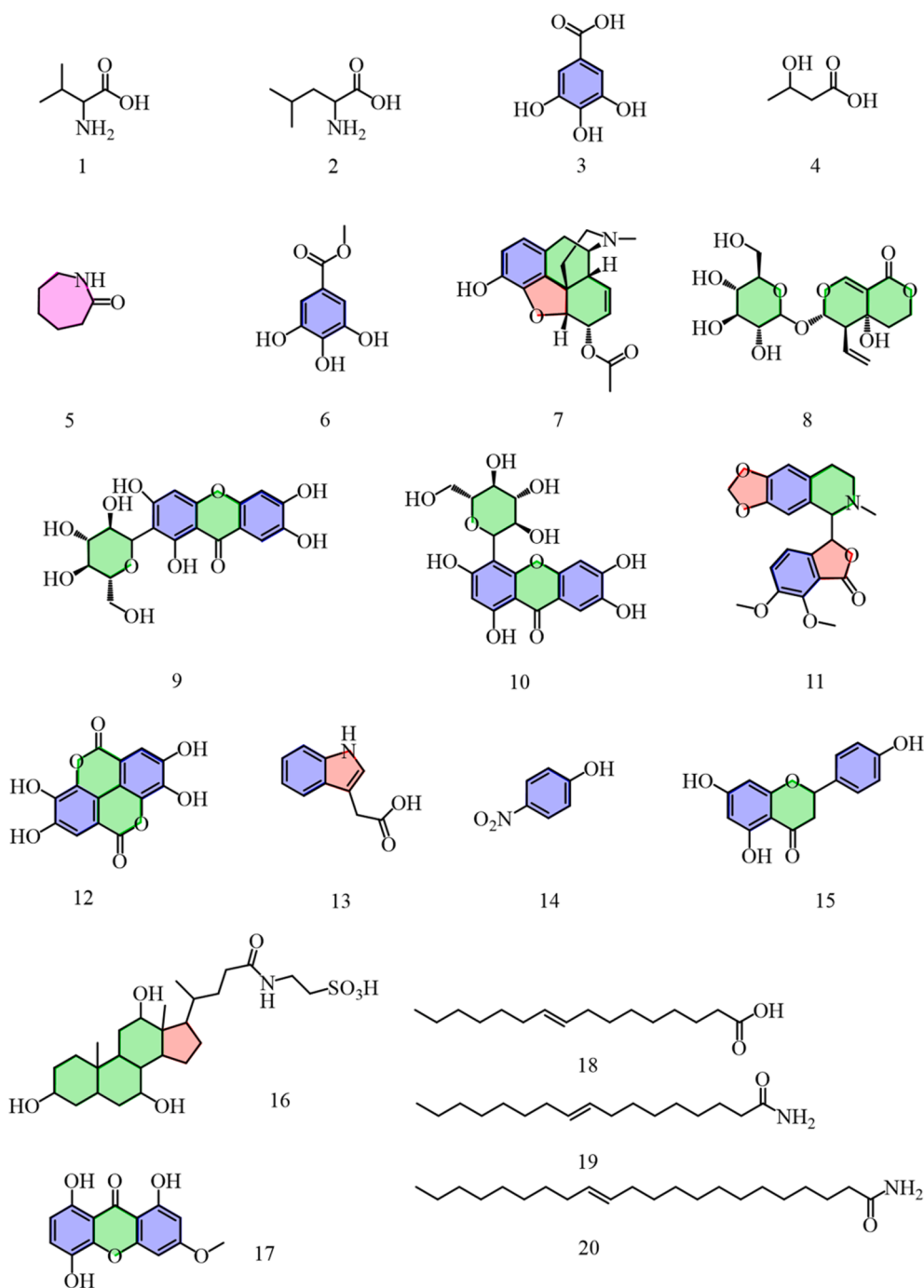
Fig. 5. The structural formula of the blood-incorporated constituents in SSP. **(1)** Valine. **(2)** Leucine. **(3)** Gallic acid. **(4)** 3-Hydroxybutyric. **(5)** Caprolactam. **(6)** Methyl gallate. **(7)** 6-Acetylmorphine. **(8)** Swertiamarin. **(9)** Mangiferin. **(10)** Isomangiferin. **(11)** Hydrastine. **(12)** Ellagic acid. **(13)** Indole-3-acetic acid. **(14)** 4-Nitrophenol. **(15)** Naringenin. **(16)** Taurocholic acid. **(17)** Bellidifolin. **(18)** Palmitoleic acid. **(19)** Oleamide. **(20)** Erucamide.

predominantly correlated with biological processes like drug response, negative regulation of apoptosis, intracellular receptor signaling pathways, and positive regulation of apoptosis. KEGG enrichment suggested apoptosis and the VEGF signaling pathway as central to SSP's CH remediation. VEGF's pivotal role in vascular formation and endothelial gene expression modulation substantiates its influence on endothelial dysfunction and hepatic fibrosis development (Apte et al., 2019, Ntellas et al., 2020). Additionally, hepatocyte-derived VEGFA has been implicated in expediting fibrosis and hepatocarcinogenesis by HSC activation during NAFLD progression (Shen, 2021).

To further decipher SSP's anti-CH modus operandi, molecular docking assessed the interaction potential between 20 systemic components-such as gallic acid, swertiamarin, ellagic acid, and bellidifolin-and five core targets (AKT1, VEGFA, CASP3, SRC, MAPK3). The analysis disclosed affirmative binding affinities, with ellagic acid demonstrating especially stable docking to MAPK3 as evidenced by the lowest binding energy. Complementarily, the therapeutic benefits of SSP in CH treatment, and its impact on the expression of the quintet of core proteins, were substantiated through HE staining and immunohistochemical approaches. HE staining results signified SSP's efficacy in mitigating inflammatory exudation and hemorrhage within hepatic tissue cells. Immunohistochemistry revealed upregulated expression of the core proteins post-ANIT gavage, while SSP treatment inversely modulated their expression. This indicates SSP's regulatory effect on the
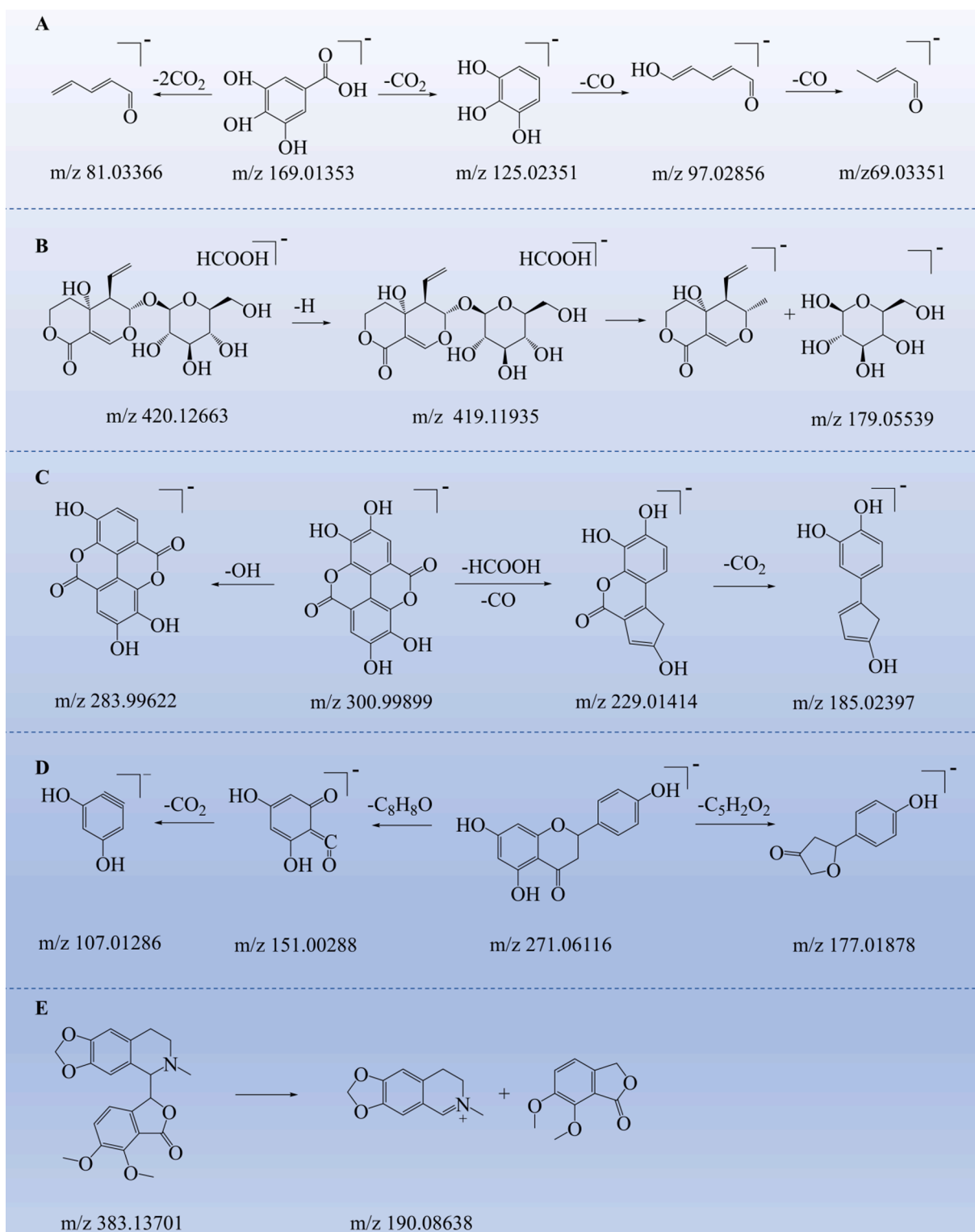
Fig. 6. The possible fragmentation pathways of the main blood-incorporated constituents in SSP. **(A)** Gallic acid. **(B)** Swertiamarin. **(C)** Ellagic acid. **(D)** Naringenin. **(E)** Hydrastine.

VEGF signaling pathway through these proteins, thus mediating its therapeutic action in CH management.

5. Conclusions

Collectively, in this study, we firstly characterized the *in vivo* and *in vitro* chemical composition of Tibetan medicine SSP using UHPLC-Q-

Exactive Orbitrap/MS technique, then investigated the blood-incorporated constituents through network pharmacology and molecular docking, and finally performed preliminary validation of key targets through *in vivo* animal experiments. We found that the main active components of SSP exerting its anti-CH effects include swertiamarin, ellagic acid, taurocholic acid and bellidifolin. These components may exert their anti-CH effects through modulation of key targets such as
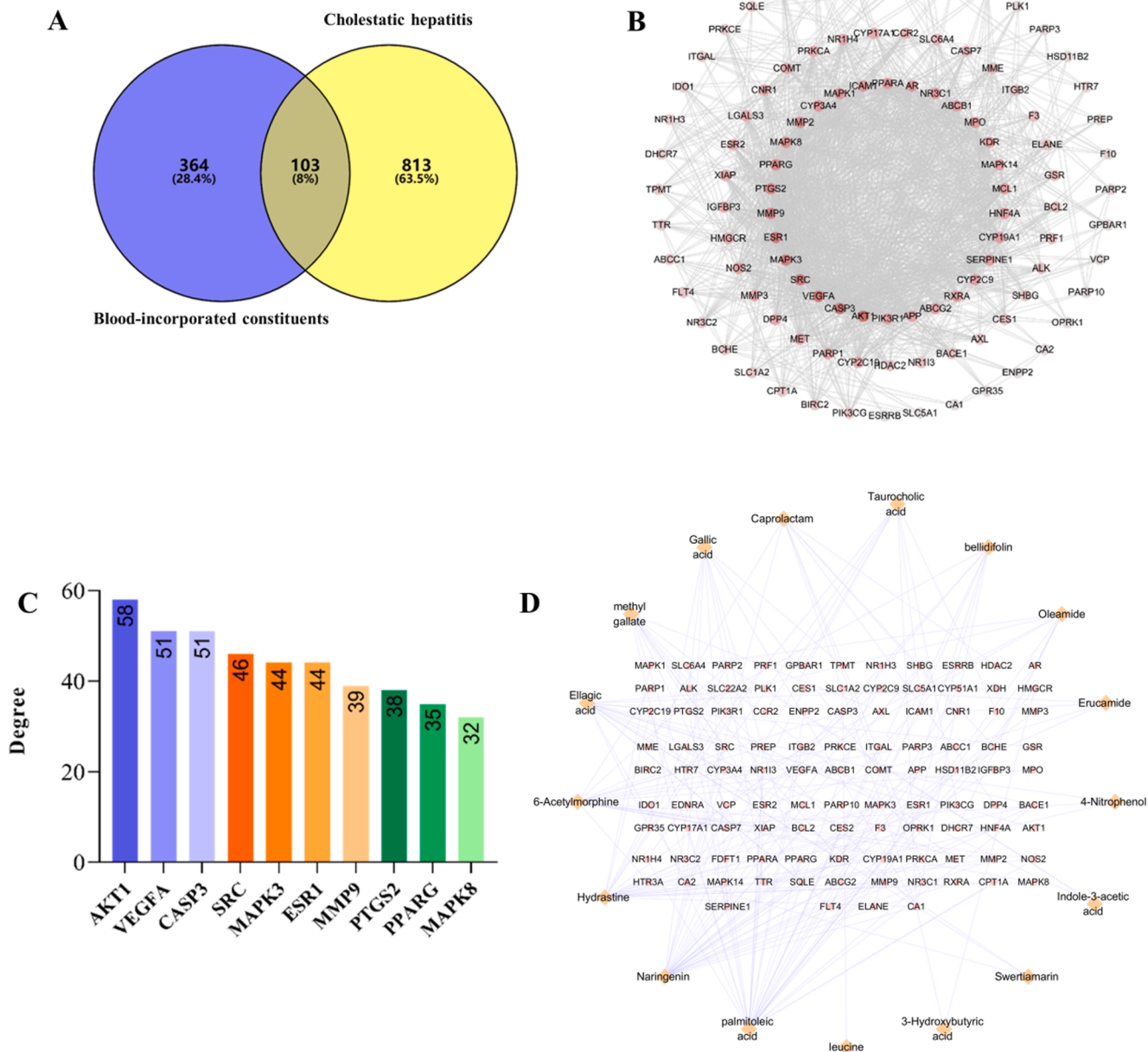
Fig. 7. The target PPI network of CH and SSP blood-entering components analysis. **(A)** Venn plots of the cross-targets between CH and the blood-incorporated constituents in SSP. **(B)** The PPI network of 103 intersection targets. **(C)** The degree value of the top 10 intersecting targets. **(D)** Visualization of the interaction network between SSP blood-incorporated constituents and 103 cross-targets drawn by Cytoscape 3.9.1. The orange square nodes represent blood-incorporated constituents of SSP and the round nodes represent targets for drug component-disease interactions. (For interpretation of the references to color in this figure legend, the reader is referred to the web version of this article.)
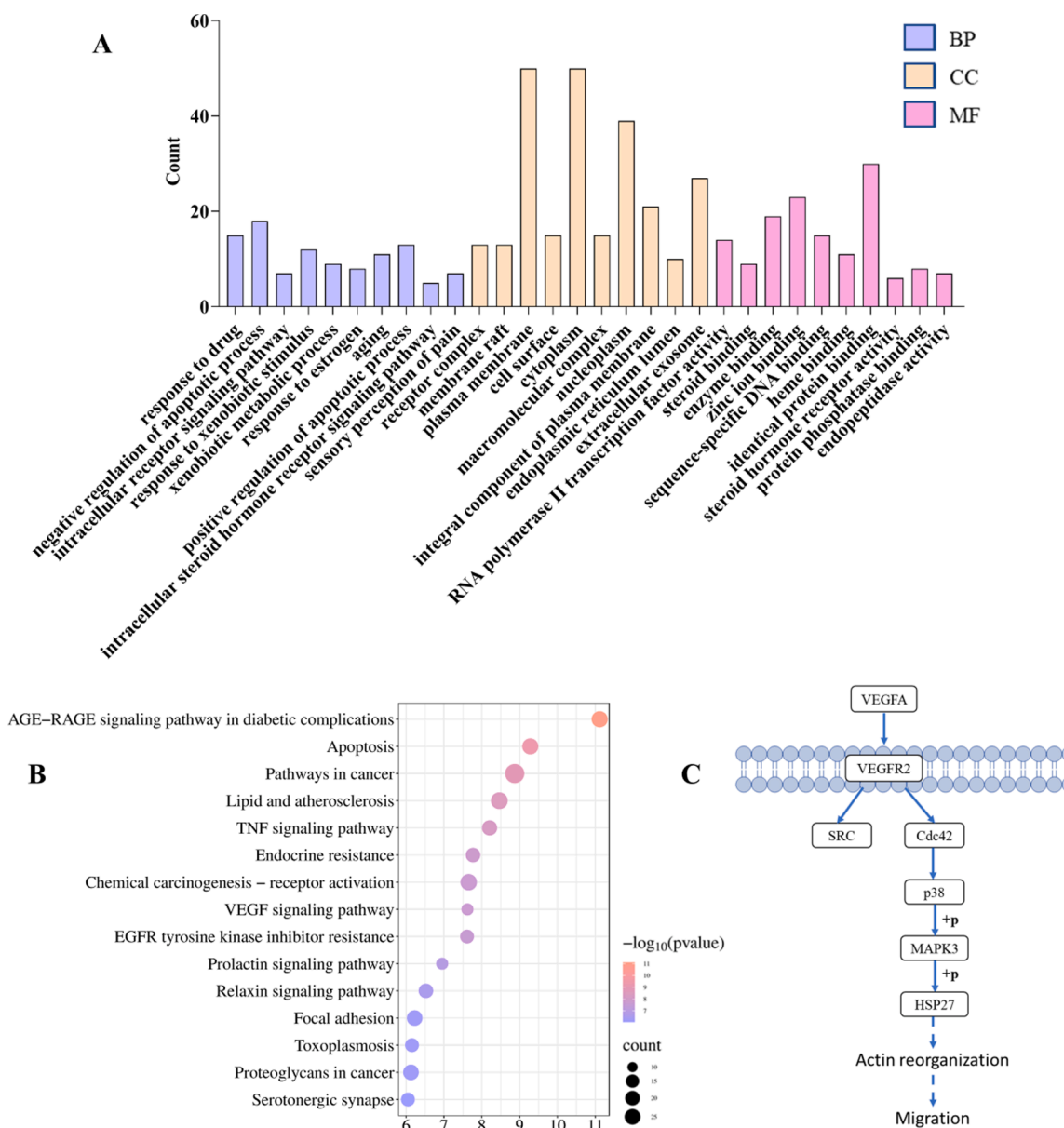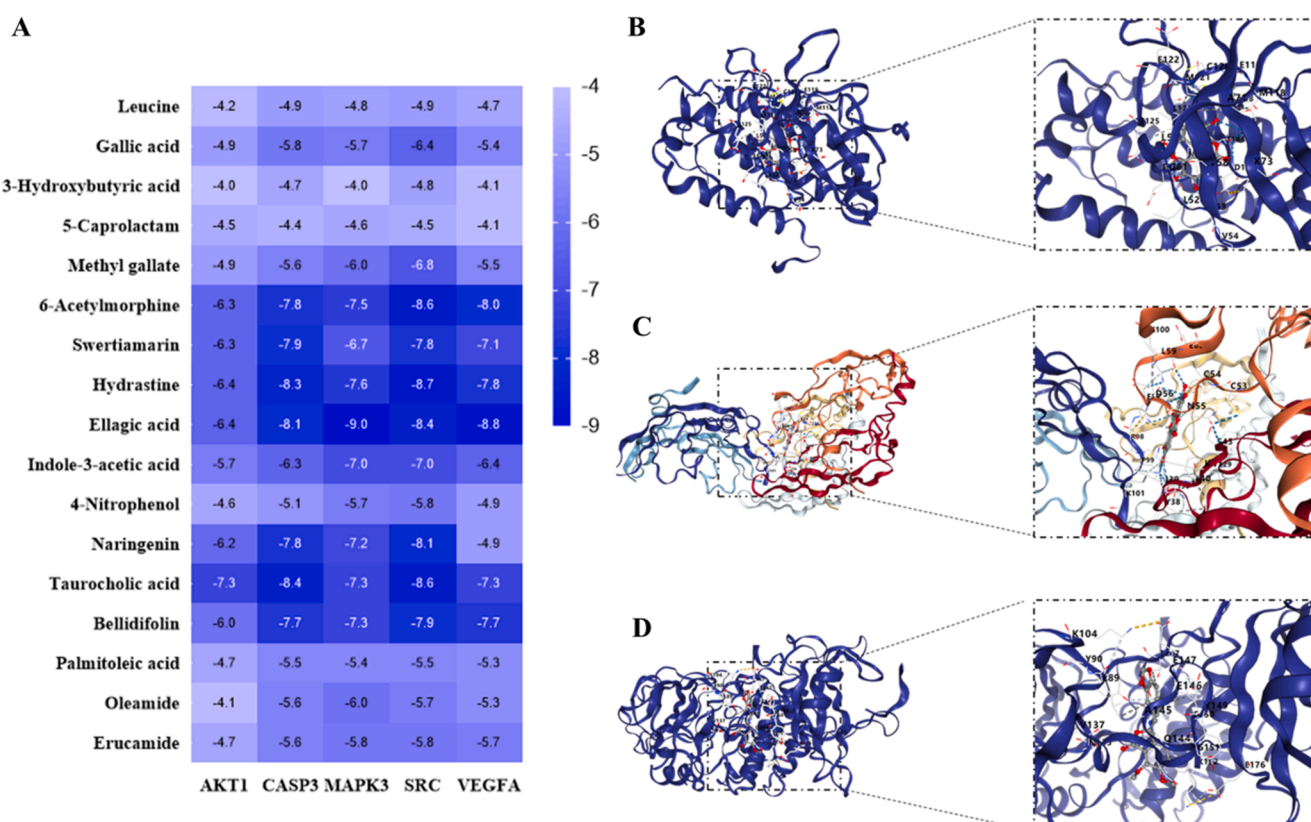
Fig. 8. GO and KEGG analysis of the core targets. **(A)** The top 10 GO terms of hub genes. **(B)** The top 15 KEGG pathway of hub genes. **(C)** VEGF signaling pathway.
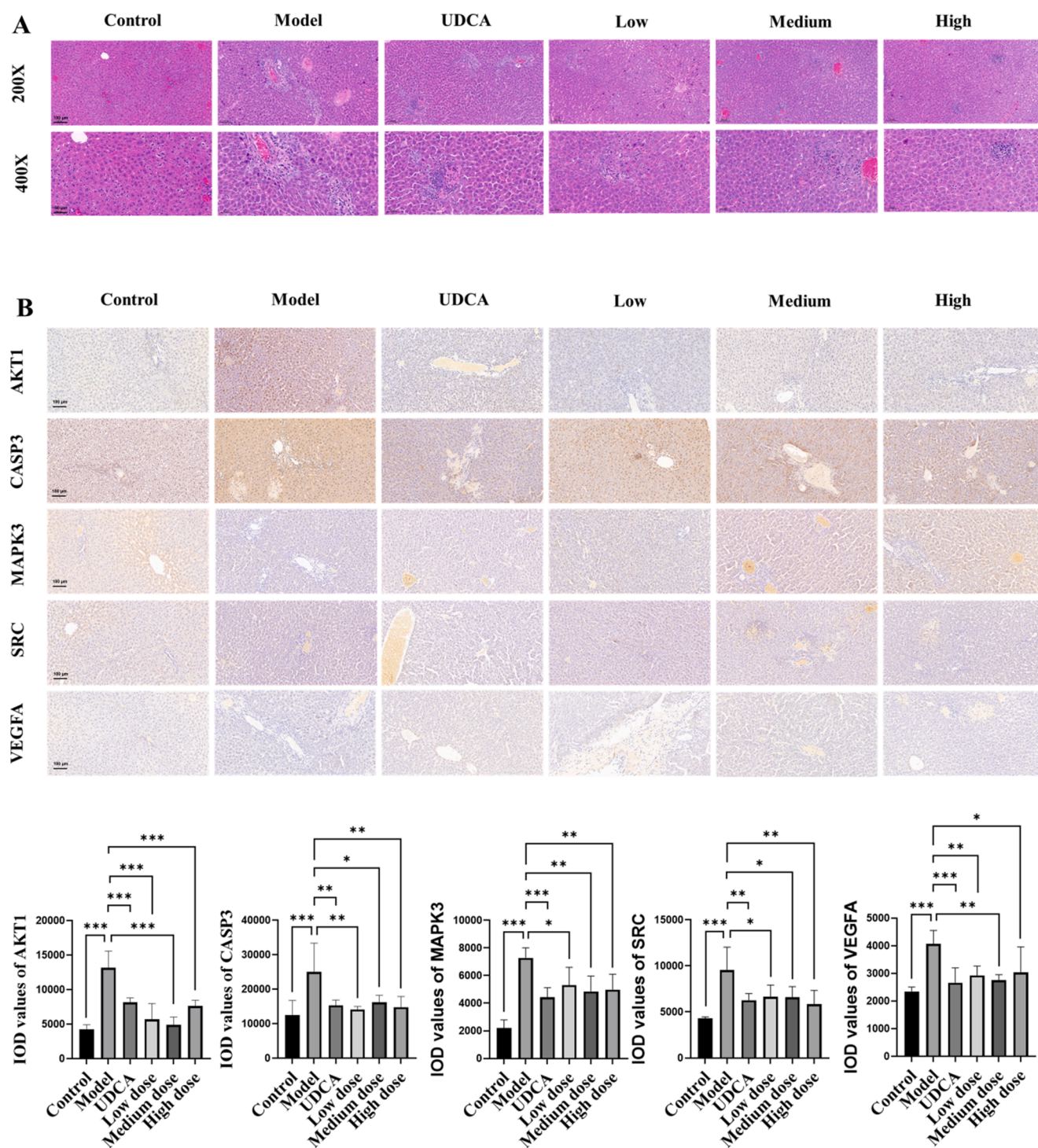
Fig. 9. Molecular docking results for the core targets. **(A)** The heat map of docking results between the core targets (including VEGFA, SRC, MAPK3, CASP3, and AKT1) and 17 blood-incorporated constituents. **(B)** Ellagic acid-MAPK3 (7NRB). **(C)** Ellagic acid-VEGFA (3QTK). **(D)** Hydrastine-SRC (1FMK).

Fig. 10. Pathological effect of SSP on CH model rats and verification of core targets. **(A)** The histopathology of liver tissue was observed by HE staining. Magnification (200×; 400 ×). **(B)** The changes in the core targets (including VEGFA, SRC, MAPK3, CASP3, and AKT1) of the SSP were detected by immunohistochemical method. Magnification (200 ×). Data were expressed as the mean ± SD (n = 3), *$p < 0.05$, **$p < 0.01$, ***$p < 0.001$.

AKT1, VEGFA, CASP3, SRC and MAPK3. It is worth noting that our current study still has some limitations and we have only assessed the anti-CH efficacy of SSP as a whole. However, whether the main active ingredients of SSP alone are also effective in the treatment of CH, as well as their direct targets and mechanisms are still key research directions that need to be strengthened in the future. Furthermore, in our investigation, the anticipated dose-dependent inhibition across varying concentrations of SSP was not observed. This counterintuitive biological response may be explained by several factors intrinsic to the multifaceted nature of herbal formulations. Pharmacokinetic complexities such as non-linear absorption, distribution, metabolism, or excretion of SSP constituents could contribute to this phenomenon. Moreover, we hypothesize the presence of a ceiling effect, wherein maximum inhibitory efficacy is reached at lower dosages, beyond which no additional suppression of target proteins is discernible. Additionally, adaptive cellular feedback mechanisms might attenuate the inhibitory effects at higher concentrations. Understanding the interplay between these components in SSP and their cumulative biological impact necessitates

further elucidation. To address this complexity, future studies will aim to dissect the pharmacological intricacies of SSP, potentially shedding light on these unexpected results and refining our comprehension of its therapeutic mechanisms in CH treatment. As a conclusion, it is hoped that this experiment will provide a reference for subsequent studies on the treatment of CH with the Tibetan medicine SSP.

CRediT authorship contribution statement

Jing Qin: Methodology, Investigation, Writing – original draft. **Gelin Xiang:** Data curation, Investigation, Visualization. **Huimin Gao:** Data curation, Investigation, Visualization. **Xianli Meng:** Supervision, Writing – review & editing, Resources. **Shaohui Wang:** Conceptualization, Supervision, Writing – review & editing, Resources. **Yi Zhang:** Conceptualization, Supervision, Writing – review & editing, Resources.

Declaration of competing interest

The authors declare that they have no known competing financial interests or personal relationships that could have appeared to influence the work reported in this paper.

Acknowledgements

References

Aabideen, Z.U., Mumtaz, M.W., Akhtar, M.T., et al., 2020. Anti-obesity attributes; UHPLC-QTOF-MS-based metabolite profiling and molecular docking insights of taraxacum officinale. Molecules 25. https://doi.org/10.3390/molecules25214935.

Abirami, A., Sinsinwar, S., Rajalakshmi, P., et al., 2022. Antioxidant and cytoprotective properties of loganic acid isolated from seeds of Strychnos potatorum L. against heavy metal induced toxicity in PBMC model. Drug Chem. Toxicol. 45, 239–249. https://doi.org/10.1080/01480545.2019.1681445.

Abu Bakar, F. I., M. F. Abu Bakar, N. Abdullah, et al., 2020. Optimization of Extraction Conditions of Phytochemical Compounds and Anti-Gout Activity of Euphorbia hirta L. (Ara Tanah) Using Response Surface Methodology and Liquid Chromatography-Mass Spectrometry (LC-MS) Analysis. Evid Based Complement Alternat Med. 2020, 4501261. 10.1155/2020/4501261.

Apte, R.S., Chen, D.S., Ferrara, N., 2019. VEGF in signaling and disease: Beyond discovery and development. Cell 176, 1248–1264. https://doi.org/10.1016/j.cell.2019.01.021.

Bai, L., Han, L., Lu, X., et al., 2017. UHPLC-MS/MS determination and pharmacokinetic study of plantamajoside in rat plasma after oral administration of single plantamajoside and Plantago asiatica extract. Biomed. Chromatogr. 31 https://doi.org/10.1002/bmc.3883.

Beszterda, M., Kasperkowiak, M., Frański, R., 2020. Comment on the published data concerning the identification of biochanin A and prunetin by LC/ESI-MS. Talanta 211, 120733. https://doi.org/10.1016/j.talanta.2020.120733.

Birkler, R.I., Stottrup, N.B., Hermannson, S., et al., 2010. A UPLC-MS/MS application for profiling of intermediary energy metabolites in microdialysis samples–a method for high-throughput. J. Pharm. Biomed. Anal. 53, 983–990. https://doi.org/10.1016/j.jpba.2010.06.005.

Boyer, J.L., 2013. Bile formation and secretion. Compr. Physiol. 3, 1035–1078. https://doi.org/10.1002/cphy.c120027.

Brito, J. A. G. d., L. d. S. Pinto, C. F. Chaves, et al., 2021. Chemophenetic Significance of Anomalocalyx uleanus Metabolites are Revealed by Dereplication Using Molecular Networking Tools. Molecules. 26, 10.3390/molecules26040925.

Bruce, S.J., Guy, P.A., Rezzi, S., et al., 2010. Quantitative measurement of betaine and free choline in plasma, cereals and cereal products by isotope dilution LC-MS/MS. J. Agric. Food Chem. 58, 2055–2061. https://doi.org/10.1021/jf903930k.

Castillo-Peinado, L.S., López-Bascón, M.A., Mena-Bravo, A., et al., 2019. Determination of primary fatty acid amides in different biological fluids by LC-MS/MS in MRM mode with synthetic deuterated standards: Influence of biofluid matrix on sample preparation. Talanta 193, 29–36. https://doi.org/10.1016/j.talanta.2018.09.088.

Chatzizacharias, N.A., Kouraklis, G.P., Giaginis, C.T., et al., 2012. Clinical significance of Src expression and activity in human neoplasia. Histol. Histopathol. 27, 677–692. https://doi.org/10.14670/hh-27.677.

Cheiran, K.P., Raimundo, V.P., Manfroi, V., et al., 2019. Simultaneous identification of low-molecular weight phenolic and nitrogen compounds in craft beers by HPLC-ESI-MS/MS. Food Chem. 286, 113–122. https://doi.org/10.1016/j.foodchem.2019.01.198.

Chen, M., Gou, L., Lu, H., 2023. The pharmacology research progress of ellagic acid online first. Modernization Trad. Chinese Med. Mater. Med. World Sci. Technol. 1–7 https://doi.org/10.11842/wst.20211115004.

Chen, K., Wu, T., Song, H., 2016. Research progress on pharmacological activities of swertiamarin. Drugs & Clinic 31, 1684–1688. https://doi.org/10.7501/j.issn.1674-5515.2016.10.040.

Cheng, M., Liu, R., Wu, Y., et al., 2016. LC-MS/MS determination and urinary excretion study of seven alkaloids in healthy Chinese volunteers after oral administration of Shuanghua Baihe tablets. J. Pharm. Biomed. Anal. 118, 89–95. https://doi.org/10.1016/j.jpba.2015.10.014.

Chithra, S., Jasim, B., Anisha, C., et al., 2014. LC-MS/MS based identification of piperine production by endophytic Mycosphaerella sp. PF13 from Piper nigrum. Appl. Biochem. Biotechnol. 173, 30–35. https://doi.org/10.1007/s12010-014-0832-3.

Choi, W.G., Kim, J.H., Kim, D.K., et al., 2018. Simultaneous determination of chlorogenic acid isomers and metabolites in rat plasma using LC-MS/MS and its application to A pharmacokinetic study following oral administration of stauntonia hexaphylla leaf extract (YRA-1909) to rats. Pharmaceutics 10. https://doi.org/10.3390/pharmaceutics10030143.

Costa, T.O., Morales, R.A., Brito, J.P., et al., 2005. Occurrence of bufotenin in the Osteocephalus genus (Anura: Hylidae). Toxicon 46, 371–375. https://doi.org/10.1016/j.toxicon.2005.02.006.

Dabur, R., Mittal, A., 2016. Detection and qualitative analysis of fatty acid amides in the urine of alcoholics using HPLC-QTOF-MS. Alcohol 52, 71–78. https://doi.org/10.1016/j.alcohol.2016.03.004.

de Souza, R.R., Bretanha, L.C., Dalmarco, E.M., et al., 2015. Modulatory effect of Senecio brasiliensis (Spreng) Less. in a murine model of inflammation induced by carrageenan into the pleural cavity. J. Ethnopharmacol. 168, 373–379. https://doi.org/10.1016/j.jep.2015.03.032.

Decker, P., Muller, S., 2002. Modulating poly (ADP-ribose) polymerase activity: potential for the prevention and therapy of pathogenic situations involving DNA damage and oxidative stress. Curr. Pharm. Biotechnol. 3, 275–283. https://doi.org/10.2174/1389201023378265.

Dou, L., Duan, L., Guo, L., et al., 2017. An UHPLC-MS/MS method for simultaneous determination of quercetin 3- O -rutinoside, kaempferol 3- O -rutinoside, isorhamnetin 3- O -rutinoside, bilobalide and ligustrazine in rat plasma, and its application to pharmacokinetic study of Xingxiong injection. Chin. J. Nat. Med. 15, 710–720. https://doi.org/10.1016/s1875-5364(17)30101-2.

Dutschke, J., Suchowski, M., Pietsch, J., 2021. Simultaneous determination of selected catechins and pyrogallol in deer intoxications by HPLC-MS/MS. J. Chromatogr. B Analyt. Technol. Biomed. Life Sci. 1180, 122886 https://doi.org/10.1016/j.jchromb.2021.122886.

[25] Expert consensus on the diagnosis and treatment of cholestatic liver disease: an update in 5. Journal of Clinical Hepatology. 31, 1563-1574. 10.3969/j.issn.1001-5256.5.10.002.

Fang, N., Yu, S., Prior, R.L., 2002. LC/MS/MS characterization of phenolic constituents in dried plums. J. Agric. Food Chem. 50, 3579–3585. https://doi.org/10.1021/jf0201327.

Fang, K., Zheng, X., Xu, L., et al., 2020. Experimental research progress of traditional Chinese medicine in the prevention and treatment of cholestatic liver disease. Chinese J. Integrated Trad. Western Med. Liver Diseases 30, 375–377. https://doi.org/10.3969/j.issn.1005-0264.2020.04.027.

Farha, A.K., Hatha, A.M., 2019. Bioprospecting potential and secondary metabolite profile of a novel sediment-derived fungus Penicillium sp. ArCSPf from continental slope of Eastern Arabian Sea. Mycology 10, 109–117. https://doi.org/10.1080/21501203.2019.1572034.

Friedman, M., Levin, C.E., Lee, S.-U., et al., 2008. Analysis by HPLC and LC/MS of pungent piperamides in commercial black, white, green, and red whole and ground peppercorns. J. Agric. Food Chem. 56, 3028–3036. https://doi.org/10.1021/jf703711z.

Ghavami, S., Cunnington, R.H., Gupta, S., et al., 2015. Autophagy is a regulator of TGF-β1-induced fibrogenesis in primary human atrial myofibroblasts. Cell Death Dis. 6, e1696.

Gill, B.D., Indyk, H.E., Kobayashi, T., et al., 2020. Comparison of LC-MS/MS and enzymatic methods for the determination of total choline and total carnitine in infant formula and milk products. J. AOAC Int. 103, 1293–1300. https://doi.org/10.1093/jaoacint/qsaa060.

Gong, J., Li, L., Lin, Y., et al., 2020. Simultaneous determination of gallic acid, methyl gallate, and 1,3,6-tri-O-galloyl-beta-d-glucose from Turkish galls in rat plasma using liquid chromatography-tandem mass spectrometry and its application to pharmacokinetics study. Biomed. Chromatogr. 34, e4916. https://doi.org/10.1002/bmc.4916.

Gu, P., Liu, R., Cheng, M., et al., 2016. Simultaneous quantification of chlorogenic acid and taurocholic acid in human plasma by LC-MS/MS and its application to a pharmacokinetic study after oral administration of Shuanghua Baihe tablets. Chin. J. Nat. Med. 14, 313–320. https://doi.org/10.1016/s1875-5364(16)30034-6.

Guan, H., Li, K., Wang, X., et al., 2017. Identification of metabolites of the cardioprotective alkaloid dehydrocorydaline in rat plasma and bile by liquid chromatography coupled with triple quadrupole linear ion trap mass spectrometry. Molecules 22. https://doi.org/10.3390/molecules22101686.

Guo, X., Cheng, M., Hu, P., et al., 2018. Absorption, metabolism, and pharmacokinetics profiles of norathyriol, an aglycone of mangiferin, in rats by HPLC-MS/MS. J. Agric. Food Chem. 66, 12227–12235. https://doi.org/10.1021/acs.jafc.8b03763.

Gupta, P.K., Barone, G., Gurley, B.J., et al., 2015. Hydrastine pharmacokinetics and metabolism after a single oral dose of goldenseal (Hydrastis canadensis) to humans. Drug Metab. Dispos. 43, 534–552. https://doi.org/10.1124/dmd.114.059410.

Han, P., Tian, D., 2016. New progress of pathogenesis and therapeutic agents of hepatic cholestasi. Chinese J. Gastroenterol. Hepatol. 25, 584–588. https://doi.org/10.3969/j.issn.1006-5709.2016.05.026.

He, J., Tian, C., Ouyang, H., et al., 2014. Determination of swertianolin in rat plasma by LC-MS/MS and its application to a pharmacokinetic study. Biomed. Chromatogr. 28, 1418–1422. https://doi.org/10.1002/bmc.3184.

Hengartner, M.O., 2000. The biochemistry of apoptosis. Nature 407, 770–776. https://doi.org/10.1038/35037710.

Hernández, F., Sancho, J.V., Pozo, O.J., 2004. An estimation of the exposure to organophosphorus pesticides through the simultaneous determination of their main metabolites in urine by liquid chromatography-tandem mass spectrometry. J. Chromatogr. B Analyt. Technol. Biomed. Life Sci. 808, 229–239. https://doi.org/10.1016/j.jchromb.2004.05.019.

Huang, X., Su, S., Cui, W., et al., 2014. Simultaneous determination of paeoniflorin, albiflorin, ferulic acid, tetrahydropalmatine, protopine, typhaneoside, senkyunolide I in Beagle dogs plasma by UPLC-MS/MS and its application to a pharmacokinetic study after Oral Administration of Shaofu Zhuyu Decoction. J. Chromatogr. B Analyt. Technol. Biomed. Life Sci. 962, 75–81. https://doi.org/10.1016/j.jchromb.2014.05.032.

Huang, X., Fan, X., Lu, M., 2023. Research progress on penthorum chinense pursh in common liver diseases. Modernization Trad. Chinese Med. Mater. Med. World Sci. Technol. 1–6 https://doi.org/10.11842/wst.20211107010.

Huang, Y., Sun, H., Qin, X., et al., 2017. A UPLC-MS/MS method for simultaneous determination of free and total forms of a phenolic acid and two flavonoids in rat plasma and its application to comparative pharmacokinetic studies of polygonum capitatum extract in rats. Molecules 22. https://doi.org/10.3390/molecules22030353.

Huang, Y., Cheng, P., Zhang, Z., et al., 2018. Biotransformation and tissue distribution of protopine and allocryptopine and effects of Plume Poppy Total Alkaloid on liver drug-metabolizing enzymes. Sci. Rep. 8, 537. https://doi.org/10.1038/s41598-017-18816-7.

Huang, M., Zhang, Y., Xu, S., et al., 2015. Identification and quantification of phenolic compounds in Vitex negundo L. var. cannabifolia (Siebold et Zucc.) Hand.-Mazz. using liquid chromatography combined with quadrupole time-of-flight and triple quadrupole mass spectrometers. J. Pharm. Biomed. Anal. 108, 11–20. https://doi.org/10.1016/j.jpba.2015.01.049.

Jia, Q., Huang, X., Yao, G., et al., 2020. Pharmacokinetic study of thirteen ingredients after the oral administration of flos chrysanthemi extract in rats by UPLC-MS/MS. Biomed. Res. Int. 2020, 8420409. https://doi.org/10.1155/2020/8420409.

Khurana, R.K., Kaur, S., Kaur, J., et al., 2017. Elucidation of stress-induced degradation products of mangiferin: Method development and validation. Biomed. Chromatogr. 31 https://doi.org/10.1002/bmc.3935.

Kim, Y.-I., Hirai, S., Takahashi, H., et al., 2011. 9-oxo-10(E),12(E)-Octadecadienoic acid derived from tomato is a potent PPAR alpha agonist to decrease triglyceride accumulation in mouse primary hepatocytes. Mol. Nutr. Food Res. 55, 585–593. https://doi.org/10.1002/mnfr.201000264.

Kumar, V., Chandra, S., 2015. LC-ESI/MS determination of xanthone and secoiridoid glycosides from in vitro regenerated and in vivo Swertia chirayita. Physiol. Mol. Biol. Plants 21, 51–60. https://doi.org/10.1007/s12298-014-0276-9.

Kumar, A., Kumar, S., Kumar, D., et al., 2014. UPLC/MS/MS method for quantification and cytotoxic activity of sesquiterpene lactones isolated from Saussurea lappa. J. Ethnopharmacol. 155, 1393–1397. https://doi.org/10.1016/j.jep.2014.07.037.

Lang, R., Yagar, E.F., Eggers, R., et al., 2008. Quantitative investigation of trigonelline, nicotinic acid, and nicotinamide in foods, urine, and plasma by means of LC/MS/MS and stable isotope dilution analysis. J. Agric. Food Chem. 56, 11114–11121. https://doi.org/10.1021/jf802838s.

Li, P., S. Liu, Q. Liu, et al., 2019. Screening of acetylcholinesterase inhibitors and characterizing of phytochemical constituents from Dichocarpum auriculatum (Franch.) W.T. Wang & P. K. Hsiao through UPLC-MS combined with an acetylcholinesterase inhibition assay in vitro. J Ethnopharmacol. 245, 112185. 10.1016/j.jep.2019.112185.

Li, Y., Feng, X., Zhang, Y., et al., 2020a. Dietary flavone from the Tetrastigma hemsleyanum vine triggers human lung adenocarcinoma apoptosis via autophagy. Food Funct. 11, 9776–9788. https://doi.org/10.1039/d0fo01997f.

Li, Y., Li, X., Gu, J., et al., 2020b. Study on protective mechanism of Tibetan medicine Ershiwuwei Songshi Pills on cholestatic liver injury in rats based on FXR signaling pathway. China J. Chinese Mater. Med. 45, 5273–5279. https://doi.org/10.19540/j.cnki.cjcmm.20200727.401.

Li, Q., Li, H., Xu, T., et al., 2018. Analysis on medication regularities of traditional Tibetan medicine treating hepatitis based on data mining. Chinese J. Ethnomed. Ethnopharm. 27, 4–7. https://doi.org/10.3969/j.issn.1007-8517.2018.12.zgmzmjyyzz201812002.

Li, Y., An, K., Sun, J., et al., 2011a. Chemical constituents of vinegar-processed Kansui radix. Food and Drug 13, 183–185. https://doi.org/10.3969/j.issn.1672-979X.2011.03.009.

Li, H., Peng, X., He, J., et al., 2011b. Development and validation of a LC-ESI-MS/MS method for the determination of swertiamarin in rat plasma and its application in pharmacokinetics. J. Chromatogr. B Analyt. Technol. Biomed. Life Sci. 879, 1653–1658. https://doi.org/10.1016/j.jchromb.2011.04.003.

Li, J., Wang, S., Wang, Y., et al., 2021. Comparative metabolism study on chlorogenic acid, cryptochlorogenic acid and neochlorogenic acid using UHPLC-Q-TOF MS coupled with network pharmacology. Chin. J. Nat. Med. 19, 212–224. https://doi.org/10.1016/s1875-5364(21)60023-7.

Li, X., Wei, S., Niu, S., et al., 2022a. Network pharmacology prediction and molecular docking-based strategy to explore the potential mechanism of Huanglian Jiedu Decoction against sepsis. Comput. Biol. Med. 144, 105389 https://doi.org/10.1016/j.compbiomed.2022.105389.

LI, C., Zhang, D., Liu, Y., et al., 2022b. Identification and attribution of chemical constituents from Erlong Capsules based on UPLC-Q-TOF-MS/MS. Chinese Traditional Patent Medicine 44, 132–141. https://doi.org/10.3969/j.issn.1001-1528.2022.01.026.

Li, W., Zhou, H., Chu, Y., et al., 2017. Simultaneous determination and pharmacokinetics of danshensu, protocatechuic aldehyde, 4-hydroxy-3-methyloxyphenyl lactic acid and protocatechuic acid in human plasma by LC-MS/MS after oral administration of Compound Danshen Dripping Pills. J. Pharm. Biomed. Anal. 145, 860–864. https://doi.org/10.1016/j.jpba.2017.06.014.

Lin, G., Chang, C., Lin, H., 2015. Systematic profiling of indole-3-acetic acid biosynthesis in bacteria using LC–MS/MS. J. Chromatogr. B 988, 53–58. https://doi.org/10.1016/j.jchromb.2015.02.025.

Lindholm, C.R., Zhang, X., Spengler, E.K., et al., 2022. Severe cholestatic hepatitis secondary to SARS-CoV-2. ACG Case Rep. J. 9, e00753. https://doi.org/10.14309/crj.0000000000000753.

Long, Y., J. Luo, M. Hu, et al., 2017. Protective effect of ellagic acid on acute liver injury induced by CCl4 in mice and its mechanism. Journal of Jilin University(Medicine Edition). 10.13481/j.1671-587x.20170321.

Lou, Y., Wu, H., Zheng, J., et al., 2020. Determination and pharmacokinetic study of skimmin by UHPLC-MS/MS in rat plasma. J. Pharm. Biomed. Anal. 179, 112969 https://doi.org/10.1016/j.jpba.2019.112969.

Luo, Y., Cui, M., Wang, H., et al., 2022. Analysis of chemical composition in different parts of fritillaria thunbergii using UHPLC-QTOF-MS/MS. Chinese J. Mod. Appl. Pharm. 39, 1984–1991. https://doi.org/10.13748/j.cnki.issn1007-7693.2022.15.011.

Ma, X., Zhang, M., Fang, G., et al., 2021. Ursolic acid reduces hepatocellular apoptosis and alleviates alcohol-induced liver injury via irreversible inhibition of CASP3 in vivo. Acta Pharmacol. Sin. 42, 1101–1110. https://doi.org/10.1038/s41401-020-00534-y.

Mantonakis, E., Giaginis, C., Pikoulis, E., et al., 2017. FAK, Src and p-Paxillin expression is decreased in liver metastasis of colorectal carcinoma patients. J. Buon. 22, 1097–1106.

Meng, X., Cai, D., Zhu, Q., et al., 2020. Rapid identification and analysis of chemical components in heartwood of Dalbergia cochinchinensis by UPLC-Q-TOF-MS/MS. Chinese J. Exp. Trad. Med. Formulae 26, 143–156. https://doi.org/10.13422/j.cnki.syfjx.20200647.

Mykhailenko, O., Korinek, M., Ivanauskas, L., et al., 2020. Qualitative and quantitative analysis of Ukrainian Iris species: A fresh look on their antioxidant content and biological activities. Molecules 25. https://doi.org/10.3390/molecules25194588.

Nie, Y., Hu, Y., Yu, K., et al., 2019. Akt1 regulates pulmonary fibrosis via modulating IL-13 expression in macrophages. Innate Immun. 25, 451–461. https://doi.org/10.1177/1753425919861774.

Ntellas, P., Mavroeidis, L., Gkoura, S., et al., 2020. Old player-new tricks: Non angiogenic effects of the VEGF/VEGFR pathway in cancer. Cancers (Basel) 12. https://doi.org/10.3390/cancers12113145.

Osna, N.A., Jr, T.M.D., Kharbanda, K.K., 2017. Alcoholic liver disease: Pathogenesis and current management. Alcohol Res. 38, 147–161.

Owen, R.W., Haubner, R., Hull, W.E., et al., 2003. Isolation and structure elucidation of the major individual polyphenols in carob fibre. Food Chem. Toxicol. 41, 1727–1738. https://doi.org/10.1016/s0278-6915(03)00200-x.

Palandra, J., Prusakiewicz, J., Ozer, J.S., et al., 2009. Endogenous ethanolamine analysis in human plasma using HPLC tandem MS with electrospray ionization. J. Chromatogr. B Analyt. Technol. Biomed. Life Sci. 877, 2052–2060. https://doi.org/10.1016/j.jchromb.2009.05.043.

Pan, L., Gao, J., Bi, R., et al., 2021. Study on quality standard of Shiwuwei Sai'erdou Pill. Chinese J. Mod. Appl. Pharm. https://doi.org/10.13748/j.cnki.issn1007-7693.2021.20.008.

Pantoja Pulido, K.D., Colmenares Dulcey, A.J., Isaza Martinez, J.H., 2017. New caffeic acid derivative from Tithonia diversifolia (Hemsl.) A. Gray butanolic extract and its antioxidant activity. Food Chem. Toxicol. 109, 1079–1085. https://doi.org/10.1016/j.fct.2017.03.059.

Parker, D.L., Rybak, M.E., Pfeiffer, C.M., 2012. Phytoestrogen biomonitoring: an extractionless LC-MS/MS method for measuring urinary isoflavones and lignans by use of atmospheric pressure photoionization (APPI). Anal. Bioanal. Chem. 402, 1123–1136. https://doi.org/10.1007/s00216-011-5550-x.

Pei, L., Liu, S., Zheng, J., et al., 2012. A sensitive method for determination of furanodiene in rat plasma using liquid chromatography/tandem mass spectrometry and its application to a pharmacokinetic study. Biomed. Chromatogr. 26, 826–832. https://doi.org/10.1002/bmc.1736.

Plaza, A., Montoro, P., Benavides, A., et al., 2005. Phenylpropanoid glycosides from Tynanthus panurensis: characterization and LC-MS quantitative analysis. J. Agric. Food Chem. 53, 2853–2858. https://doi.org/10.1021/jf0479867.

Qin, J., Zhang, Y., Qi, M., et al., 2016. Rapid analysis of compounds in leaves of Chinese seabuckthorn and Tibetan seabuckthorn by UPLC / Q-TOF-MS. China J. Chinese Mater. Med. 41, 1461–1468. https://doi.org/10.4268/cjcmm20160816.

Qu, J., Chen, W., Luo, G., et al., 2002. Rapid determination of underivatized pyroglutamic acid, glutamic acid, glutamine and other relevant amino acids in fermentation media by LC-MS-MS. Analyst 127, 66–69. https://doi.org/10.1039/b108422b.

Reinehr, R., Sommerfeld, A., Häussinger, D., 2013. The Src family kinases: distinct functions of c-Src, Yes, and Fyn in the liver. Biomol. Concepts 4, 129–142. https://doi.org/10.1515/bmc-2012-0047.

Ren, H., Cui, X., Hu, J., et al., 2021. Analysis on chemical constituents in rhizomes of Bergenia scopulosa by UHPLC-Q exactive focus MS/MS enhanced publishing. Chinese J. Exp. Trad. Med. Formulae 27, 118–128. https://doi.org/10.13422/j.cnki.syfjx.20210146.

Ruiz-Colon, K., Martinez, M.A., Silva-Torres, L.A., et al., 2012. Simultaneous determination of xylazine, free morphine, codeine, 6-acetylmorphine, cocaine and benzoylecgonine in postmortem blood by UPLC-MS-MS. J. Anal. Toxicol. 36, 319–326. https://doi.org/10.1093/jat/bks024.

Sharma, A., Sharma, R., Kumar, D., et al., 2020. Berberis lycium Royle fruit extract mitigates oxi-inflammatory stress by suppressing NF-kappaB/MAPK signalling cascade in activated macrophages and Treg proliferation in splenic lymphocytes. Inflammopharmacology 28, 1053–1072. https://doi.org/10.1007/s10787-018-0548-z.

Shen, H., 2021. The Role of Hepatocyte-derived VEGFA in Liver Regeneration and Non-alcoholic Fatty Liver Disease. Doctor, Naval Medical University.

Sheng, N., Yuan, L., Zhi, X., et al., 2014. Application of a liquid chromatography-tandem mass spectrometry method to the pharmacokinetics, tissue distribution and excretion studies of sweroside in rats. J. Chromatogr. B Analyt. Technol. Biomed. Life Sci. 969, 1–11. https://doi.org/10.1016/j.jchromb.2014.07.042.

Shi, F., Pan, H., Lu, Y., et al., 2018. An HPLC-MS/MS method for the simultaneous determination of luteolin and its major metabolites in rat plasma and its application to a pharmacokinetic study. J. Sep. Sci. 41, 3830–3839. https://doi.org/10.1002/jssc.201800585.

Song, W., Kim, N., Kim, S., et al., 2009. Liquid chromatography-tandem mass spectrometry for the determination of jaceosidin in rat plasma. J. Pharm. Biomed. Anal. 49, 381–386. https://doi.org/10.1016/j.jpba.2008.10.021.

Steiner, I., Brauers, G., Temme, O., et al., 2016. A sensitive method for the determination of hordenine in human serum by ESI(+) UPLC-MS/MS for forensic toxicological applications. Anal. Bioanal. Chem. 408, 2285–2292. https://doi.org/10.1007/s00216-016-9324-3.

Sun, M., Wang, H., Ding, F., et al., 2020. Qualitative analysis of flavonoids in tetrastigma hemsleyanum based on UPLC-quadrupole/exactive orbitrap mass spectrometry and mass defect filter method. J. Chinese Mass Spectrometry Soc. 41, 359–367. https://doi.org/10.7538/zpxb.2019.0064.

Sun, X., Zhang, P., Wu, X., et al., 2014. Simultaneous determination of calycosin-7-O-beta-d-glucoside, calycosin, formononetin, astragaloside IV and schisandrin in rat plasma by LC-MS/MS: application to a pharmacokinetic study after oral administration of Shenqi Wuwei chewable tablets. Biomed. Chromatogr. 28, 1118–1125. https://doi.org/10.1002/bmc.3128.

Sun, Z., 2016. Study on Active Ingredients from Penthorum Chinense Pursh. Master Master, Chongqing University.

Tafzi, N., Woillard, J.B., Fleytoux, A., et al., 2020. Phenotyping of uracil and 5-fluoro-uracil metabolism using LC-MS/MS for prevention of toxicity and dose adjustment of fluoropyrimidines. Ther. Drug Monit. 42, 540–547. https://doi.org/10.1097/ftd.0000000000000768.

Taherkhani, A., Khodadadi, P., Samie, L., et al., 2023. Flavonoids as strong inhibitors of MAPK3: A computational drug discovery approach. Int. J. Anal. Chem. 2023, 8899240. https://doi.org/10.1155/2023/8899240.

Tian, X., Li, Z., Lin, Y., et al., 2014a. Study on the PK profiles of magnoflorine and its potential interaction in Cortex phellodendri decoction by LC-MS/MS. Anal. Bioanal. Chem. 406, 841–849. https://doi.org/10.1007/s00216-013-7530-9.

Tian, C., Zhang, T., Wang, L., et al., 2014b. The hepatoprotective effect and chemical constituents of total iridoids and xanthones extracted from Swertia mussotii Franch. J. Ethnopharmacol. 154, 259–266. https://doi.org/10.1016/j.jep.2014.04.018.

Vaidya, A., Singh, S., Limaye, L., et al., 2019. Chimeric feeders of mesenchymal stromal cells and stromal cells modified with constitutively active AKT expand hematopoietic stem cells. Regen. Med. 14, 535–553. https://doi.org/10.2217/rme-2018-0157.

Virág, D., Király, M., Drahos, L., et al., 2020. Development, validation and application of LC-MS/MS method for quantification of amino acids, kynurenine and serotonin in human plasma. J. Pharm. Biomed. Anal. 180, 113018 https://doi.org/10.1016/j.jpba.2019.113018.

Wang, Z., Wu, Q., Yu, Y., et al., 2015. Determination and pharmacokinetic study of four xanthones in rat plasma after oral administration of Gentianella acuta extract by UHPLC-ESI-MS/MS. J. Ethnopharmacol. 174, 261–269. https://doi.org/10.1016/j.jep.2015.08.023.

Wang, Z., Song, M., Cui, B., et al., 2019. A LC-MS/MS method for simultaneous determination of seven alkaloids in rat plasma after oral administration of Phellodendri chinensis cortex extract and its application to a pharmacokinetic study. J. Sep. Sci. 42, 1351–1363. https://doi.org/10.1002/jssc.201801018.

Wang, R., Xiong, X., Yang, M., et al., 2020. A pharmacokinetics study of orally administered higenamine in rats using LC-MS/MS for doping control analysis. Drug Test. Anal. 12, 485–495. https://doi.org/10.1002/dta.2756.

Wang, W., Yan, P., Yang, B., 2021. Study on fragmentation patterns of coumarins in Notopterygium inchum with ultrahigh performance liquid chromatography combined with quadrupole time-of-flight mass spectrometry. China J. Chinese Mater. Med. 46, 1179–1190. https://doi.org/10.19540/j.cnki.cjcmm.20201012.203.

Wang, L., 2021. Qualitative Analysis and in vivo metabolic profile study of Lagotis brachystachys Maxim based on UPLC-Q-TOF-MS technolog Master, Jiangxi University of Chinese Medicine.

Wu, H., Chen, G., Wang, J., et al., 2020. TIM-4 interference in Kupffer cells against CCL4-induced liver fibrosis by mediating Akt1/Mitophagy signalling pathway. Cell Prolif. 53, e12731.

Wu, Y., Lin, L., Sung, J.S., et al., 2006. Determination of acteoside in Cistanche deserticola and Boschniakia rossica and its pharmacokinetics in freely-moving rats using LC-MS/MS. J. Chromatogr. B Analyt. Technol. Biomed. Life Sci. 844, 89–95. https://doi.org/10.1016/j.jchromb.2006.07.011.

Wu, Y., Wu, M.L., Lin, C., et al., 2012. Determination of caprolactam and 6-aminocaproic acid in human urine using hydrophilic interaction liquid chromatography-tandem mass spectrometry. J. Chromatogr. B Analyt. Technol. Biomed. Life Sci. 885–886, 61–65. https://doi.org/10.1016/j.jchromb.2011.12.014.

Xie, H., Yang, J., Feng, S., et al., 2015. Simultaneous quantitative determination of sanguinarine, chelerythrine, dihydrosanguinarine and dihydrochelerythrine in chicken by HPLC-MS/MS method and its applications to drug residue and pharmacokinetic study. J. Chromatogr. B Analyt. Technol. Biomed. Life Sci. 985, 124–130. https://doi.org/10.1016/j.jchromb.2015.01.001.

Xie, J., Zhang, L., Zeng, J., et al., 2017. Fast identification of constituents of Lagotis brevituba by using UPLC-Q-TOF-MS/MS method. Zhongguo Zhong Yao Za Zhi 42, 2123–2136. https://doi.org/10.19540/j.cnki.cjcmm.20170307.012.

Xiong, P., Li, K., Gong, K., et al., 2021. Identification of chemical constituents in the Kadsura Coccinea Fructus based on UHPLC-Q-exactive orbitrap MS. China Pharmaceuticals 30, 55–60. https://doi.org/10.3969/j.issn.1006-4931.2021.18.014.

Xu, B., Yang, G., Ge, S., et al., 2013. Validated LC-MS/MS method for the determination of 3-hydroxflavone and its glucuronide in blood and bioequivalent buffers: application to pharmacokinetic, absorption, and metabolism studies. J. Pharm. Biomed. Anal. 85, 245–252. https://doi.org/10.1016/j.jpba.2013.07.030.

Xu, B., Li, P., Zhang, G., 2015. Comparative pharmacokinetics of puerarin, daidzin, baicalin, glycyrrhizic acid, liquiritin, berberine, palmatine and jateorhizine by liquid chromatography-mass spectrometry after oral administration of Gegenqinlian decoction and active components alignment (ACA) to rats. J. Chromatogr. B Analyt. Technol. Biomed. Life Sci. 988, 33–44. https://doi.org/10.1016/j.jchromb.2015.01.039.

Xu, D., Zhang, G., Zhang, T., et al., 2020. Pharmacokinetic comparisons of naringenin and naringenin-nicotinamide cocrystal in rats by LC-MS/MS. J. Anal. Methods Chem. 2020, 8364218. https://doi.org/10.1155/2020/8364218.

Yan, L., Yin, P., Ma, C., et al., 2014. Method development and validation for pharmacokinetic and tissue distributions of ellagic acid using ultrahigh performance liquid chromatography-tandem mass spectrometry (UPLC-MS/MS). Molecules 19, 18923–18935. https://doi.org/10.3390/molecules191118923.

Yang, L., Wang, X., Xu, Y., et al., 2017. Simultaneous determination of anemoside B4, phellodendrine, berberine, palmatine, obakunone, esculin, esculetin in rat plasma by UPLC-ESI-MS/MS and its application to a comparative pharmacokinetic study in normal and ulcerative colitis rats. J. Pharm. Biomed. Anal. 134, 43–52. https://doi.org/10.1016/j.jpba.2016.11.021.

Yang, T., Wang, G., 2021. Efficacy of the combination of ademetionine 1,4 - butanedisulfonate for injection in the treatment of patients with cholestatic hepatitis. Heilongjiang Med. Pharm. 44, 109–110.

Yang, L., Yang, L., Jia, P., et al., 2016. HPLC-Q-TOF-MS/MS-based analysis of chemical constituents in Choerospondiatis fructus. J. Second Military Med. Univ. 37, 159–166. https://doi.org/10.16781/j.0258-879x.2016.02.0159.

Yao, N., Huang, Y., Li, X., et al., 2020. Study on the fingerprint chromatography of bran atractylodis macrocephalae rhizoma dispensing granules. Asia-Pac. Trad. Med. 16, 78–83. https://doi.org/10.11954/ytctyy.202012022.

Yao, J., Sun, J., Wu, L., et al., 2017. Identification of major constituents from propolis by LC-IT-TOF-MS. J. China Pharma. Univ. 48, 178–183. https://doi.org/10.11665/j.issn.1000-5048.20170208.

Yilmaz, M.A., Ertas, A., Yener, I., et al., 2018. A comprehensive LC-MS/MS method validation for the quantitative investigation of 37 fingerprint phytochemicals in Achillea species: A detailed examination of A. coarctata and A. monocephala. J. Pharm. Biomed. Anal. 154, 413–424. https://doi.org/10.1016/j.jpba.2018.02.059.

Yu, J., 2017. Analysis of Polyphenols in Camellia Nitidissima Chi Master, Guangxi University of Traditional Chinese Medicine.

Zeng, Y., Li, S., Wang, X., et al., 2015. Validated LC-MS/MS method for the determination of scopoletin in rat plasma and its application to pharmacokinetic studies. Molecules 20, 18988–19001. https://doi.org/10.3390/molecules201018988.

Zhang, J., Chen, M., Ju, W., et al., 2010. Liquid chromatograph/tandem mass spectrometry assay for the simultaneous determination of chlorogenic acid and cinnamic acid in plasma and its application to a pharmacokinetic study. J. Pharm. Biomed. Anal. 51, 685–690. https://doi.org/10.1016/j.jpba.2009.09.039.

Zhang, C., Z. Zheng, D. Wang, et al., 2021. Analysis of Chemical Constituents from Calyxes of Physalis alkekengi var. franchetii by UPLC-Q-Orbitrap HRMS. Journal of Chinese Medicinal Materials. 2600-2608. 10.13863/j.issn1001-4454.2021.11.017.

Zhang, Q., Ford, L.A., Goodman, K.D., et al., 2016a. LC-MS/MS method for quantitation of seven biomarkers in human plasma for the assessment of insulin resistance and impaired glucose tolerance. J. Chromatogr. B Analyt. Technol. Biomed. Life Sci. https://doi.org/10.1016/j.jchromb.2016.10.025.

Zhang, X., Li, P., Guo, S., et al., 2018a. Quantitation of beta-carboline and quercetin in alligator weed (Alternanthera philoxeroides (Mart.) Griseb.) by LC-MS/MS and evaluation of cardioprotective effects of the methanol extracts. Drug Discov. Ther. 12, 341–346. https://doi.org/10.5582/ddt.2018.01070.

Zhang, C., Ma, W., Zhang, Y., et al., 2018b. Pharmacokinetics, bioavailability, and tissue distribution study of angoroside C and its metabolite ferulic acid in rat using UPLC-MS/MS. Front. Pharmacol. 9, 1186. https://doi.org/10.3389/fphar.2018.01186.

Zhang, W., Tam, H.T.B., Chen, W., et al., 2002. Studies on the structure and activity of phenylic compounds from Erigeron brev iscapus. Chin. Pharm. J. 21–24 https://doi.org/10.3321/j.issn:1001-2494.2002.08.007.

Zhang, L., Teng, L., Gong, C., et al., 2013. Simultaneous determination of harmine, harmaline and their metabolites harmol and harmalol in beagle dog plasma by

UPLC-ESI-MS/MS and its application to a pharmacokinetic study. J. Pharm. Biomed. Anal. 85, 162–168. https://doi.org/10.1016/j.jpba.2013.07.019.

Zhang, L., Cheng, Y., Du, X., et al., 2015. Swertianlarin, an herbal agent derived from swertia mussotii franch, attenuates liver injury, inflammation, and cholestasis in common bile duct-ligated rats. Evid. Based Complement. Alternat. Med. 2015, 948376 https://doi.org/10.1155/2015/948376.

Zhang, S., Xie, Y., Wang, J., et al., 2017. Development of an LC-MS/MS method for quantification of two pairs of isomeric flavonoid glycosides and other ones in rat plasma: Application to pharmacokinetic studies. Biomed. Chromatogr. 31 https://doi.org/10.1002/bmc.3972.

Zhang, Q., Xun, Y., Yang, J., 2016b. Protective effect of ellagic acid on liver injury in rats with alcoholic fatty liver and its effect on TNF-α and Leptin. Chinese Trad. Patent Med. 38, 1821–1824. https://doi.org/10.3969/j.issn.1001-1528.2016.08.033.

Zhang, R., Zhu, X., Bai, H., et al., 2019. Network pharmacology databases for Traditional Chinese Medicine: Review and assessment. Front. Pharmacol. 10, 123. https://doi.org/10.3389/fphar.2019.00123.

Zhao, L., Mehmood, A., Soliman, M.M., et al., 2021. Protective effects of ellagic acid against alcoholic liver disease in mice. Front. Nutr. 8, 744520 https://doi.org/10.3389/fnut.2021.744520.

Zheng, X., J. Yang and Y. Yang, 2016. Research progress on pharmacological effects of gallic acid. Chinese Journal of Hospital Pharmacy. 37, 94-98+102. 10.13286/j.cnki.chinhosppharmacyj.2017.01.22.

Zhou, D., Lv, D., Zhang, H., et al., 2021. Quantitative analysis of the profiles of twelve major compounds in Gentiana straminea Maxim. Roots by LC-MS/MS in an extensive germplasm survey in the Qinghai-Tibetan plateau. J. Ethnopharmacol. 280, 114068 https://doi.org/10.1016/j.jep.2021.114068.

Zhou, J., Qi, H., 2017. Simultaneous determination of eight components in radix scrophulariae by HPLC-MS/MS. Mod. Chinese Med. 19, 670–674. https://doi.org/10.13313/j.issn.1673-4890.2017.5.015.

Zhu, L., Y. LI and X. LI, 2020. Preliminary Study on Serum Medicinal Chemistry of Tibetan Medicine Bawei Chenxiang Powder based on UPLC-Q-Exactive Technology. Journal of Chinese Medicinal Materials. 43, 88-94. 10.13863/j.issn1001-4454.2020.01.018.

Zou, Q., Gu, Y., Lu, R., et al., 2013. Development of an LC/MS/MS method in order to determine arctigenin in rat plasma: its application to a pharmacokinetic study. Biomed. Chromatogr. 27, 1123–1128. https://doi.org/10.1002/bmc.2916.